Invited Review Article

Italian carbonatite system: From mantle to ore-deposit

Francesco Stoppa[a,*], Mariangela Schiazza[a], Gianluigi Rosatelli[a], Francesca Castorina[b,f], Victor V. Sharygin[c,d,e], Francesco Antonio Ambrosio[a], Noemi Vicentini[a]

[a] Department of Psychology, Health and Territory Sciences, G. d'Annunzio University of Chieti-Pescara, Italy
[b] Department of Earth Science, Sapienza University, Rome, Italy
[c] V.S. Sobolev Institute of Geology and Mineralogy SB RAS, Prospect Koptyuga 3, Novosibirsk 630090, Russia
[d] Novosibirsk State University, Pirogova Rd. 2, Novosibirsk 630090, Russia
[e] Institute of Physics and Technology, Ural Federal University, Mira Rd. 2, Ekaterinburg 620002, Russia
[f] CNR Istituto di Geologia Ambientale e Geoingegneria, Italy

ABSTRACT

A new discovery of carbonatites at Pianciano, Ficoreto and Forcinelle in the Roman Region demonstrates that Italian carbonatites are not just isolated, mantle xenoliths-bearing, primitive diatremic rocks but also evolved subtype fluor-calciocarbonatite ($F \sim 10$ wt%) associated with fluor ore ($F \sim 30$ wt%). New data constrain a multi-stage petrogenetic process, 1-orthomagmatic, 2-carbothermal, 3-hydrothermal. Petrography and geochemistry are conducive to processes of immiscibility and decarbonation, rather than assimilation and crystal fractionation. A CO_2-rich, ultra-alkaline magma is inferred to produce immiscible melilite leucitite and carbonatite melts, at lithospheric mantle depths. At the crustal level and in the presence of massive CO_2 exsolution, decarbonation reactions may be the dominant processes. Decarbonation consumes dolomite and produces calcite and periclase, which, in turn, react with silica to produce forsterite and Ca silicates (monticellite, melilite, andradite). Under carbothermal conditions, carbonate breakdown releases Sr, Ba and LREE; F and S become concentrated in residual fluids, allowing precipitation of fluorite and barite, as well as celestine and anhydrite. Fluor-calciocarbonatite is the best candidate to exsolve fluids able to deposit fluor ore, which has a smaller volume. At the hydrothermal stage, REE concentration and temperature dropping allow the formation of $LREEF^{2+}$ and $LREECO^{3+}$ ligands, which control the precipitation of interstitial LREE fluorcarbonate and silicates: (bastnäsite-(Ce), $Ce(CO_3)F$ and britholite-(Ce), $(Ce,Ca)_5(SiO_4,PO_4)_3(OH,F)$. Vanadates such as wakefieldite-(Ce), $CeVO_4$, vanadinite, $Pb_5(VO_4)_3Cl$ and coronadite $Pb(Mn_6^{4+} Mn_2^{3+})O_{16}$ characterise the matrix. At temperatures of $\leq 100\,°C$ analcime, halloysite, quartz, barren calcite, and zeolites (K-Ca) precipitate in expansion fractures, veins and dyke aureoles.

1. Introduction

Since the pioneering overview into Italian carbonatites by Stoppa and Woolley (1997), a number of new carbonatite outcrops have been discovered. Consequently, there is a need to address new outcrops and new data in a general petrogenetic model that combines and explains, consistently, old and new findings. The newly discovered carbonatites are in fact different from the mantle debris-bearing, primitive calcio-carbonatites occurring in diatremes described by Stoppa and Woolley (1997). They are evolved rocks, without mantle debris, characterised by high concentrations of LREE, Y, V, Pb, As and Cs and the presence of abundant fluorite and barite.

Fluor-calciocarbonatites occur in central Italy in a large volcanic area, named 'Roman Region' (RR) by Washington (1906) (Fig. 1). Locardi (1990) made the first mention of carbonatite magmatism in the RR and this has recently been re-evaluated by Stoppa et al. (2016). RR is 60–70 km to the West of the small monogenic carbonatitic-kamafugitic volcanoes of San Venanzo, Cupaello, Polino and Oricola (Fig. 1). Considering the different tectonic setting and specific peralkaline rock-type association and specific mineralogy (Lavecchia et al., 2006; Sharygin et al., 1996, 2013; Stoppa et al., 1997; Stoppa and Lupini, 1993; Stoppa and Schiazza, 2013, 2014), Lavecchia and Stoppa (1996) grouped them all in a different igneous province, the Intermountain Ultra-alkaline Province (IUP). Shortly after, Stoppa and Principe (1998)
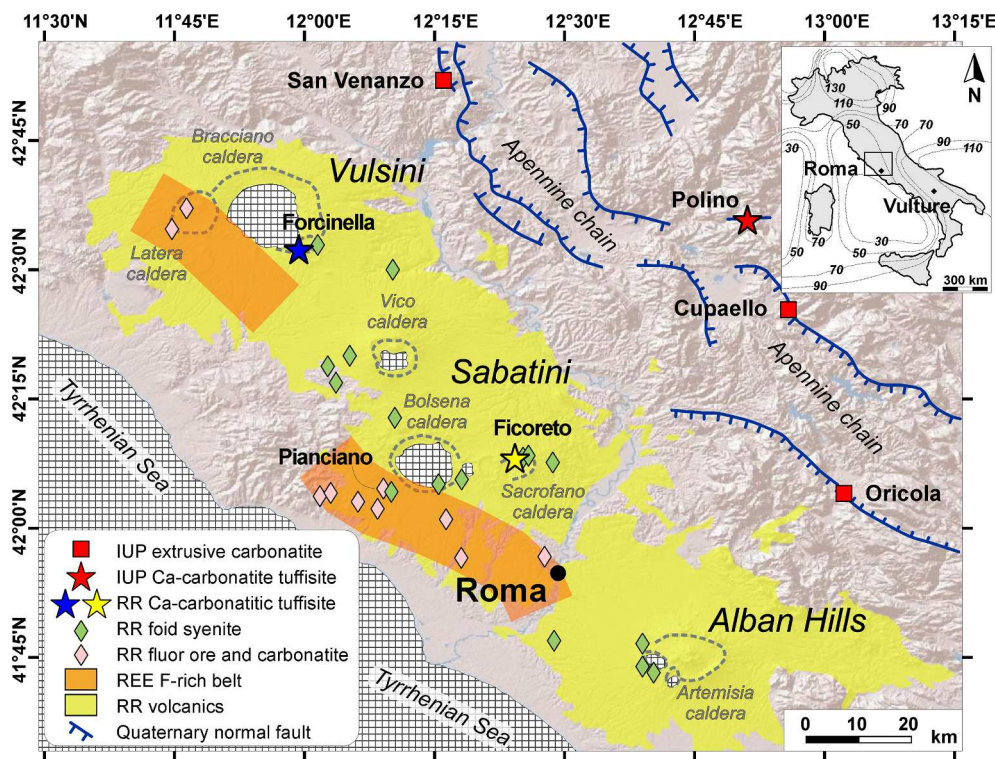

Fig. 1. Sketch map of the Roman Region (in yellow) and IUP volcanic centres (red boxes and red stars). The figure shows extrusive REE – fluor-calciocarbonatite belt (in orange, main outcrops pink diamonds), carbonatitic tuffisites (blue and yellow stars) and foid syenite ejecta (green diamonds) occurrences. Only larger calderas (dotted lines) with calderic lakes are reported among volcano landforms. The figure reports toponyms cited in the text. All symbols are in the figure. Software Q-GIS v. 2.8 (https://qgis.org/it/site/). Inset at the right top corner: Lithosphere-Asthenosphere boundary (LAB) depth contour lines, the area of Fig. 1 is indicated by a box. Tectonic and structural data from Lavecchia and Stoppa (1996) and Lavecchia et al. (2017).

provided the first description of extrusive carbonatites containing nyerereite, $Na_2Ca(CO_3)_2$, at the Vulture volcano (Stoppa et al., 2009). IUP carbonatites are generally silicocarbonatites having SiO_2 ~20 wt% and modal carbonate > 50 vol%. These rocks are probably consanguineous but distinct from RR carbonatites.

A peculiarly notable, textural mode of occurrence of IUP and RR carbonatites is a variety of tuffisites (Francis, 1989), which is here defined as a natural mixture of carbonatite droplets or carbonatitic, concentric-shelled lapilli cored by ultramafic silicate crystals, emplaced as subvolcanic tuff in dykes and diatremes (Stoppa et al., 2003). Carbonatitic tuffisites can erupt as lapilli tuff aprons around maar-diatreme systems (Stoppa, 1996). Massive microporphyritic fluor-calciocarbonatites (lava-like) associated with large fluor ore deposits are only of the RR.

The petrological data are indicative of a mantle origin for the Italian carbonatite parental melt. Italian carbonatites present a potentially compelling challenge to the petrological policies instituted after the Daily and Rittman theory of limestone assimilation (Peccerillo, 2016). In fact, all the carbonate occurrences appear to be in textural and chemical equilibrium with the silicate phases and are inferred to have a primary magmatic origin (Di Battistini et al., 2001; Martin et al., 2012).

In this paper, we detail the petrography and geochemistry (including isotopes and radiometric dating) of three carbonatitic outcrops from the RR, including two in situ tuffisite occurrences plus a large volume of microporphyritic fluor-calciocarbonatite and associated fluor ore (Fig. 1). We compare new data with the updated panorama of Italian carbonatites. The paper focuses on the presentation of a new model based on immiscibility and decarbonation. The mass of new data allows us to hypothesize petrogenetic processes that go from high to low temperature processes. We suggest that decarbonation reactions are as important as typical carbonatite processes, such as immiscibility. In addition, we propose a mechanism of evolution for the carbonatitic system and ore-precipitation. Knowledge of the mechanism of REE precipitation, speciation and the role of carbothermal/hydrothermal fluids in the formation of economic deposits is important, due to the increasing market demand for critical metals (Wall, 2013; Goodenough et al., 2016). At the moment, the Italian extrusive carbonatites having

REEs values < 1% are not of economic interest (i.e. not REE carbonatites according to Jones et al., 2013), whereas they might be of interest at these low concentrations as a by-product of fluorite production. This would require specific knowledge of the mineral compositions and a different processing route for the fluor ore that is actively quarried, which are discussed elsewhere (Al-Ali et al., 2019). However, our petrogenetic model indicates that subvolcanic complexes can host potentially economically critical metals deposits, as seen in similar geological conditions to those in RR, such as China (Hou et al., 2015; Liu and Hou, 2017) and India (Viladkar et al., 2019).

2. Roman region carbonatite occurrences

Subvolcanic carbonatites occur at Forcinella and Ficoreto and extrusive carbonatites are widespread on the west side of RR volcanoes (Fig. 1). RR carbonatites are associated with hundreds of millions of tonnes of fluor ore deposits (Mastrangelo, 1976; Stoppa et al., 2016) (Fig. 1).

The Forcinella outcrop is approximately 2 km south of the town of Montefiascone, within the Vulsini district. The outcrop is a partially eroded, small diatreme located near the shoreline of the Bolsena Lake, next to the large maar of Montefiascone. The Forcinella tuffisite consists of nucleated, concentric-shelled lapilli of carbonatitic melilite leucitite set in a very fine-grained matrix of Sr-rich calcite, analcime, barite, britholite-(Ce), baritocelestine and Ba-Ca zeolites (Fig. 2a). Melilite leucitite lapilli show rounded or amoeboid calcite globules having the same composition as the carbonate matrix of the tuffisite (Fig. 2e). Analcime and halloysite almost completely replace leucite, but fine details of the original texture are preserved. Veinlets of fluorite, harmotome, calcite and barite testify to a late hydrothermal deposition. Melilite leucitite lavas, dated from 0.28 to 0.22 Ma, surround the tuffisite (Brocchini et al., 2000).

Ficoreto is located 1.5 km ESE of Campagnano Romano town on the northern rim of the Sacrofano caldera in the Sabatini District. Ficoreto is a leucitite scoria and lava cone, dated to 0.200 ± 0.020 Ma (sample FIC06, Table 3a). The scoria cone is topped by a paleosol which, in turn, is covered by ash lapilli fall-out and late pumice-ash phonolitic
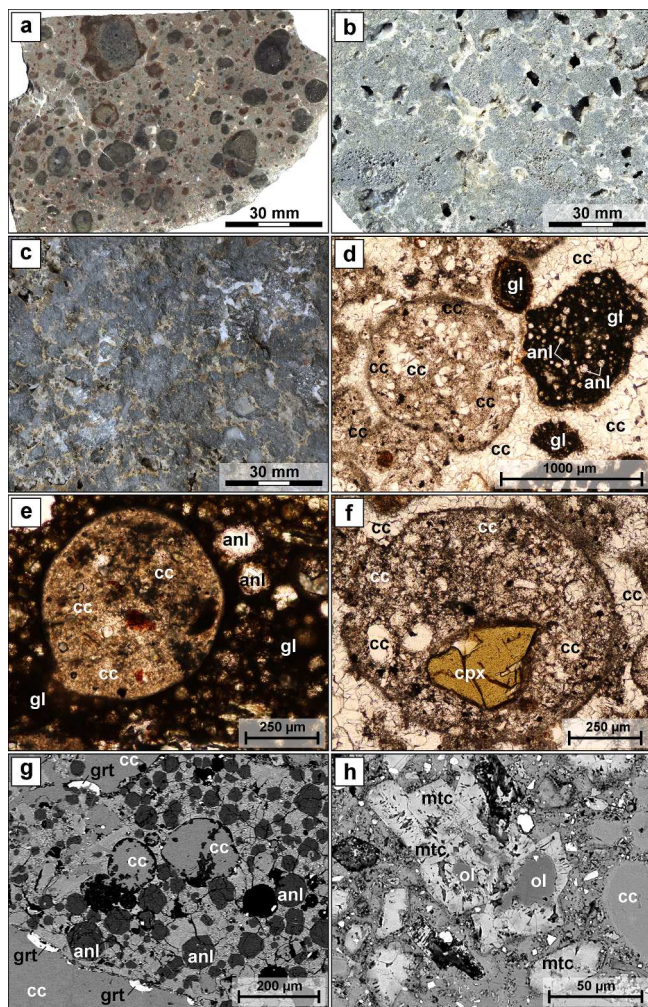
Fig. 2. Hand-scale samples and thin sections of Italian carbonatite tuffisites (stars in Fig. 1). Mineral abbreviation: cc = calcite, cpx = clinopyroxene, grt = garnet, anl = analcime, mtc = monticellite, ol = olivine, gl = glass. a) Polished sample of Forcinella carbonatitic tuffisite showing melilite leucitite concentric-lapilli set in a carbonatite groundmass (sample MF1703, of Table 1). b) Ficoreto calciocarbonatite tuffisite showing agglutinated calciocarbonatite lapilli cemented by sparry calcite (sample FIC05a of Table 1). c) Polino carbonatite tuffisite showing monticellite silicocarbonatite lapilli cemented by sparry calcite (PO2/3). d) Optical microscope image of carbonatite (left) and leucitite (right) ash droplets in carbonatitic tuffisite (FIC05d), // polarized light. e) Optical microscope image of carbonate globules hosted in a leucitite lapillus from Ficoreto (FIC01), // polarised light. Calcite laths, Sr-rich microcrystalline calcite, Sr-rich barite, fluorite, fluor and hydroxylapatite, magnetite, monticellite, vanadinite, hydrated Ca-Ce-vanadate and bastnäsite-(Ce) form the micro-porphyritic texture. f) Optical microscope image of porphyritic carbonatite pelletoidal ash with a kernel of clinopyroxene fragments, showing calcite laths in a microcrystalline groundmass of Sr-carbonate, analcime, barite, britholite-(Ce), fluorite from sample FIC05d. // polarised light. g) SEM image of a Ficoreto leucitite lapillus immersed in a microcrystalline carbonate matrix (FIC05b). Note the garnet reaction rim and the carbonate globules. h) SEM image of Polino carbonatite showing monticellite euhedra on relict forsterite core in a Sr-REE rich microcrystalline groundmass with microphenocrysts of Th-Zr-perovskite, Zr-schorlomite, REE-Sr apatite, Ti-magnetite and Cr-phlogopite xenocrysts (PO2-5).

pyroclastic flows (< 0.1 Ma). Calciocarbonatite lapilli, cemented by sparry calcite (tuffisite), fill a vent structure approximately 30 m in diameter, as described by Cozzupoli et al. (1976) (Fig. 2b). This rock is very similar to Polino tuffisite (Fig. 2c, h) described by Stoppa and Lupini (1993). A complex fracture network, associated with carbonatite dykes, crosscuts the cone. Ca-Ba zeolites and calcite infiltrate the scoria layers for several decimetres on the side of the dykes. In addition, there are many satellite dykelets of carbonatite microbreccia or soft, colloform quartz-zeolite-halloysite deposits. Carbonatite breccia has a fine-grained, turbid carbonate matrix, which suspends carbonatite and leucitite lapilli (Fig. 2b, d). The carbonatite lapilli are porphyritic and show 1 mm long laths or pseudo-hexagonal euhedra of calcite. Often they are cored by a mafic crystal kernel (Fig. 2f). Pseudo-hexagonal calcite is likely to be pseudomorph of aragonite (Hurai et al., 2013). Microcrystalline groundmass contains Sr-rich barite, fluorite, fluorapatite, hydroxylapatite, fluorellestadite, vanadinite, coronadite, bastnäsite-(Ce), magnetite and siderite. Rare accessory phases include galena, pyrite, sphalerite, monticellite, witherite and unidentified Ca-Ce-vanadates. The groundmass contains abundant globules of Sr-rich calcite with inclusions of a hydrated Ca-Ce-vanadate, strontianite, fluorapatite and hydroxylapatite (Fig. 2e). Leucitite lapilli are composed of leucite/analcime, anorthite, diopside, Ti-rich andradite, Ba-rich fluorphlogopite, titanite, fluorapatite, and Ti-rich magnetite. Andradite locally rims the lapilli at the contact with the carbonate groundmass (Fig. 2g).

The Pianciano extrusive fluor-calciocarbonatite outcrop is 20 km west of Ficoreto (Stoppa et al., 2016) (Fig. 1). The deposit comprises fluor-calciocarbonatite dykes and small cryptodomes, which intrude an overlying, plastically deformed fluor ore deposit (Fig. 3a). The volume of fluor-calciocarbonatite is much greater than that of fluor ore. Pervasive veins of halloysite plus zeolites and hydroxide-sulphides crosscut the deposit. A deeply altered and mineralised leucitite tuff occurs at the top and at the bottom of the sequence, which is up to 10 m thick (Fig. 3a). A charcoal-rich paleosol coats the original morphology. A > 10 m thick leucitite pyroclastic flow, dated 0.214 ± 0.010 Ma, tops the paleosol (sample PIA12, Table 3a). Trachyte, foid syenite, hornfels and skarn ejecta are noticeable components of the pyroclastic flow. Fluor-calciocarbonatite is porphyritic and consists of abundant calcite, occurring as laths, and pseudo-hexagonal micro phenocrysts (up to 100–200 μm) (Fig. 3b, c) set in a fluorite, calcite, barite, apatite and periclase cryptocrystalline groundmass. In particular, the pseudo-hexagons of calcite are identical to those of the Ficoreto rocks (Fig. 3b). Moreover, discrete cleavage fragments of K-feldspar, Ti-rich phlogopite, Ti-rich magnetite, titanite and diopside (up to 1 mm diameter) occur in the groundmass. Accessory phases are fluorapatite, fluorellestadite, Ba-Ca zeolites and hydrated varieties of Ca-Ce-vanadates, wakefieldite, hollandite- and alunite-supergroup minerals, celestine, siderite, quartz and vanadinite (Fig. 3d). Rare accessory phases are anhydrite, portlandite, Na-K-sulphates, galena, pyrite, sphalerite hellandite-(Ce) and scheelite.

3. Results

Twelve new analyses of RR carbonatites and seventeen new analyses of associated silicate rocks provide complete geochemistry including thirteen new stable and radiogenic isotope data with two radiometric dates; these are given in Tables 1–3. Conventional chemical diagrams for igneous rocks are not suitable for carbonatites and statistical analysis is preferred. The Rank Entropy (H) Analysis (RHA) is an informatics language that can be used to describe, group and organise the composition of objects of any nature (Petrov and Moshkin, 2015; Petrov et al., 2016; PETROS-3 software package). The RHA system calculates three parameters: R – Rank formula, H – Entropy, A – Anentropy. Software 'Petros-3' outputs gave three main statistical discriminating factors in terms of their atomic wt% (supplementary data): F + C + Ca, Si + Al + Na + K, and Mg + Fe + P. The triangular diagram, built with these factors, separates groups of rock-types into two broad different petrogenetic lineages (Fig. 4). The F + C + Ca corner accounts for calcite and fluorite, the Si + Al + Na + K corner accounts for the felsic component, and the Mg + Fe + P corner accounts for the rest of the mafic minerals. Diopside, monticellite and apatite bridge the lower corner and left corner at some distance from the axis, whereas
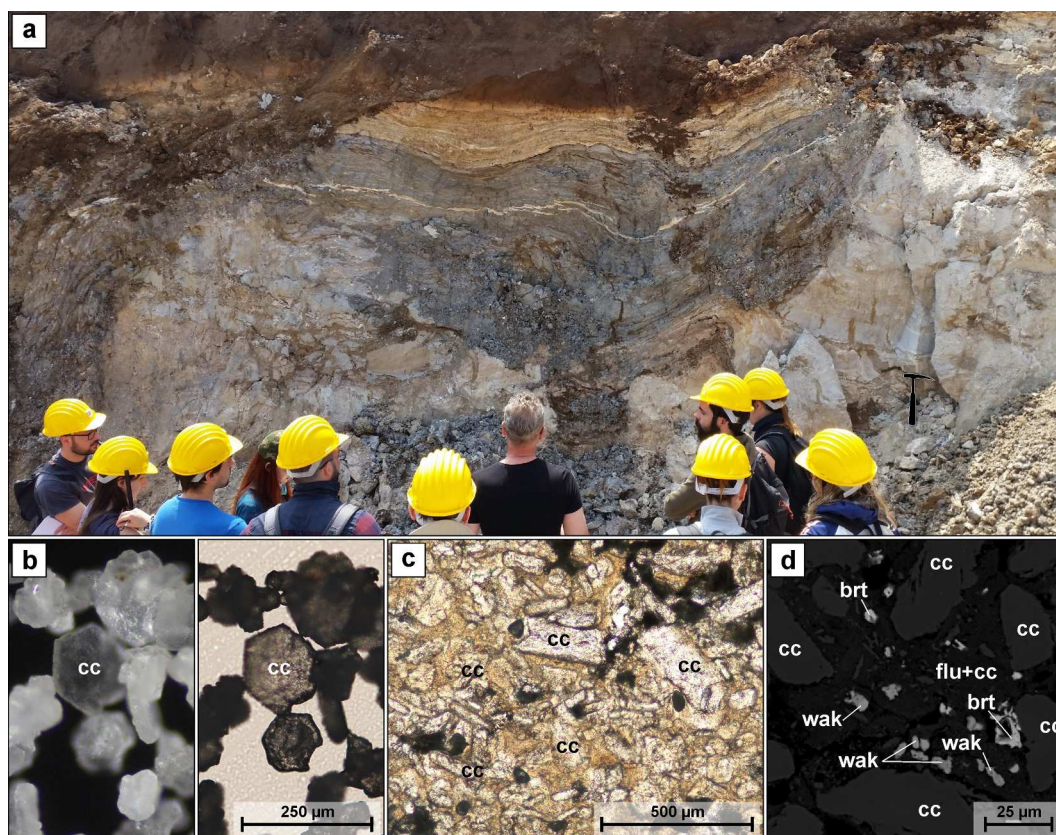
Fig. 3. Pianciano a) General view of fluor ore layers (top centre) overlaying two fluor calciocarbonatite blocks (on the left and the right). b) Optical microscope image of pseudo-hexagonal calcite (after aragonite) (PIA06). Reflected and // polarised transmitted light. c) Fluor-calciocarbonatite showing calcite laths immersed in a micro-crypto crystalline groundmass of fluorite, barite, periclase and REE-V-Pb-Mn phases (dark amoeboid patches) (PIA06). d) Back-scattered SEM image of PIA06 showing a very fine-grained groundmass of calcite, fluorite, barite and wakefieldite. Symbols: cc - calcite; brt - barite; wak - wakefieldite; flu - fluorite.

phlogopite bridges the lower corner to the right corner, but is located closer to the axis due to the relatively low F levels in this mineral. Fluorite and K-feldspars are important toward the upper left and right corners, respectively. The compositions of relevant mantle and experimental carbonatitic liquids are also plotted for comparison (Sweeney, 1994 and references therein). Ideally, the primary mantle melt is located where the standard lithosphere mantle adiabat intercepts the line linking mantle composition and primary mantle carbonatites. The PETROS output gives a notional composition, corresponding to a CO_2-rich magma, which converts into oxide percentages given the following figures: SiO_2 24.2, TiO_2 0.42, Al_2O_3 1.63, Fe_2O_3tot. 7.29, MgO 29.1, CaO 11.8, MnO 0.06, K_2O 1.87, Na_2O 2.22, P_2O_5 0.32, and CO_2 21.1 (silicomagnesiocarbonatite)

Plotting first order factors, F + C + Ca and Si + Al + Na + K, against second order factors, La-Ce-V-(Ba/100) and Rb-Zr-Nb, the studied compositions form a positive correlation curve (Fig. 5a and b). Carbonatites have a high La-Ce-V (Ba/100)/F + C + Ca ratio and associated mafic silicate rocks have a high Rb-Zr-Nb/Si + Al + Na + K ratio.

The magnesium number $Mg\#$ ($100*Mg/Mg + Fe^{2+}$) is consistently high in primitive Italian carbonatites, with an average of 71 and maximum of 95. The Cr + Ni/$Mg\#$ diagram shows that mantle-debris-bearing rocks, e.g. Polino carbonatite, plot separately from the other examples, having a Cr + Ni content up to 1100 ppm (Fig. 6a). Pb and V strongly correlate with LILE and Zn, As, U, LREE and Y (Fig. 6b and c). The highest values are from fluor-calciocarbonatites and fluor ore, whereas Italian primitive carbonatites have relatively low Pb, V (with the exception of VLT, Vallone Toppo del Lupo carbonatite from Vulture volcano), REE and U (Fig. 6c). Vanadium in Italian carbonatites averages 175 ppm (36–494 ppm), in between the extrusive and intrusive worldwide carbonatites, respectively with averages of 155 ppm

(18–383 ppm) for extrusive and 136 ppm (20–642) for intrusive.

The combined ratios of Hf, Zr, Ta, Y, and Nb vs Yb show a positive correlation and lie along a narrow mantle array, defined by Pearce (2008) for primitive middle ocean ridge basalts (MORB) and ocean island basalts (OIB) (Fig. 7a–d). Carbonatite and kimberlite extend the MORB and OIB range towards higher values of these 'immobile' pair ratios. Italian ultra-alkaline rocks generally lie between OIB and kimberlites and match general carbonatite composition, but the associated carbonatites may show considerable deviations of the $HFSE^{4+5+}$ vs HREE ratios.

Fig. 8 illustrates the primitive mantle-normalised ($_{PM}$) multi-elements and chondrite-normalised ($_{CN}$) REE variations of RR carbonatites. As a whole, Pianciano and Ficoreto carbonatitic rocks and fluor ore show a similar distribution with Large Ion Lithophile Elements (LILE: Cs, Pb, U, Ba) at approximately 1000 to 10.000_{PM} when compared to the primitive mantle, with a negative spike of K, Rb, Hf and Th (Fig. 8a, c). Arsenic is higher in Pianciano, by one order of magnitude in comparison with Ficoreto. La, Ce, and Sr are between 100 and 1000_{PM}. Ta-Nb and Zr-Hf form negative spikes. Transition metals are between 1 and 10_{PM} (Eu, Y, Zn, Sc and V). Compatible elements (Co, Ni and Cr) are between 0.001 and 0.01 units. Pianciano fluor-calciocarbonatite and fluor ore have a parallel trend, with fluor ore having a substantially higher trace element content. Ficoreto calciocarbonatite dyke rock has higher Pb and Cs and lower Ba, Th, Nb, Ta, P, As, La, Ce and Sr compared to calciocarbonatite tuffisite. In terms of REE, three main patterns are apparent at the Pianciano outcrop: fluor-calciocarbonatite, fluor ore and tuffs (7b). La is up to 5000_{CN} in fluor ore, 1500_{CN} in fluor-calciocarbonatite and tuff. The average La_{CN}/Yb_{CN} ratio figures for the three facies are 3088, 1350, and 92 units, respectively. LREE crossover between hydrothermal rocks and fluor-calciocarbonatite occurs at Pr, indicating high concentrations of LREE in fluor ore and fluor-

Table 1

Twelve new whole rock analyses of carbonatites from Roman Region of Italy. Major oxides in wt%, trace elements in ppm. LOI = mass loss on ignition. Analyses carried out at Activation Laboratories (www.actlabs.com). Rock compositions correspond to those of the rock-type groups in Fig. 3. Key letters and symbols refer to the compositional field in Fig. 3.

# analyses	PIA05	PIA06	PIA07	PIA02	PIA03	PIA04	FIC03	FIC04	FIC05a	FIC05b	FIC05d	MF1703
locality	Pianciano	Pianciano	Pianciano	Pianciano	Pianciano	Pianciano	Ficoreto	Ficoreto	Ficoreto	Ficoreto	Ficoreto	Forcinella
rock-type	(1)	(1)	(1)	(2)	(2)	(2)	(3)	(3)	(3)	(3)	(3)	(4)
litho-facies	tuff	tuff	tuff	tuff	tuff	tuff	dyke	dyke	tuffisite	tuffisite	tuffisite	tuffisite
SiO2 (wt%)	1.57	0.64	1.54	4.82	8.00	1.94	10.2	2.39	23.7	19.8	2.64	28.3
TiO2	0.02	0.01	0.03	0.09	0.13	0.03	0.18	0.05	0.40	0.34	0.04	0.61
Al2O3	0.87	0.18	0.47	1.65	3.21	0.77	2.96	0.70	6.74	5.63	0.87	10.0
Fe2O3	0.41	0.01	0.13	1.31	2.01	0.52	1.94	0.57	3.49	2.87	0.46	6.32
FeO	0.10	0.20	0.40	0.50	0.10	0.10	0.20	0.20	0.70	0.60	2.64	0.80
MnO	0.07	0.03	0.12	0.15	0.26	0.20	0.11	0.09	0.07	0.06	0.04	0.14
MgO	0.15	0.11	0.21	0.58	0.53	0.15	2.28	1.28	3.39	2.84	0.60	3.95
CaO	55.2	56.9	55.6	53.3	46.8	49.7	45.9	52.1	33.1	36.6	53.2	25.7
Na2O	0.09	0.06	0.06	0.19	0.27	0.21	0.12	0.02	2.70	2.31	0.17	0.28
K2O	0.07	0.05	0.10	0.48	0.35	0.11	0.66	0.06	0.45	0.34	0.10	0.61
P2O5	0.52	0.25	0.59	2.43	1.71	2.97	1.16	1.17	0.33	0.29	0.51	0.66
CO2	30.5	30.4	31.6	3.89	0.46	0.34	30.9	37.8	21.0	24.7	38.7	11.5
S	0.27	0.25	0.30	0.39	0.43	0.52	0.31	0.39	0.02	0.02	n.d.	n.d.
F	8.65	8.65	8.17	29.0	26.7	30.8	0.65	0.81	0.14	0.13	n.d.	n.d.
LOI	1.37	1.32	2.44	5.66	-0.46	6.06	1.94	1.61	3.00	2.61	1.36	10.6
SrO	0.52	0.56	0.58	0.53	0.44	0.19	0.93	1.12	0.14	0.16	0.18	0.27
BaO	2.51	2.96	0.35	7.89	10.05	12.06	0.27	0.26	0.07	0.06	0.03	0.44
Total	**102.9**	**102.6**	**102.7**	**112.9**	**101.0**	**106.6**	**100.7**	**100.6**	**99.4**	**99.3**	**101.5**	**100.2**
O = F	3.64	3.64	3.44	12.21	11.24	12.97	0.27	0.34	0.06	0.05	—	—
Total	**99.2**	**99.0**	**99.2**	**100.7**	**89.7**	**93.6**	**100.4**	**100.2**	**99.3**	**99.3**	**101.5**	**100.2**
Mg#	72.8	49.5	48.3	67.4	90.4	72.8	95.3	91.9	89.6	89.4	28.8	89.8
V (ppm)	128	76	161	438	384	235	183	164	150	122	92	221
Sc	0.62	0.16	0.72	1.64	2.06	0.44	6	1	15	13	2	10
Cr	< 0.5	< 0.5	15.0	< 0.5	23.4	23	20	< 20	50	40	< 20	20
Co	< 0.1	< 0.1	4.8	< 0.1	9.6	< 0.1	5	< 1	14	11	< 1	22
Ni	2.0	< 1	2.0	6	7	2	30	20	50	40	< 20	50
Cu	6.0	1.0	41.0	98	26	9	40	40	20	20	20	80
Zn	53	55	140	418	243	209	< 30	< 30	< 30	< 30	< 30	80
As	181	115	186	545	565	508	26	35	13	9	15	25
Rb	< 10	< 10	< 10	220	110	< 10	52	6	524	428	55	153
Sr	4378	4751	4939	4474	3706	1629	7862	9442	1146	1363	1500	2257
Y	8.0	8.0	8.0	15	16	15	28	24	16	14	12	35
Zr	15.0	27.0	12.0	43	68	21	82	19	186	157	24	345
Nb	24.0	13.0	31.0	94	64	40	23	29	8	6	12	19
Cs	< 0.2	7.0	9.9	< 0.2	51.4	53.1	4.8	0.9	38	27.9	6.2	51.8
Ba	22440	26520	3155	70710	89970	108000	2428	2295	615	535	300	3949
Hf	< 0.2	< 0.2	< 0.2	< 0.2	< 0.2	< 0.2	1.7	0.4	4.7	4	0.5	6.5
Ta	< 0.3	< 0.3	< 0.3	< 0.3	< 0.3	< 0.3	0.6	0.5	0.4	0.3	0.2	0.7
Pb	380.0	150.0	676.0	1010	780	492	85	111	752	535	702	111
W	76.0	33.0	< 1	504	194	159	25	23	2	2	5	6
Th	2.8	0.9	2.6	7.2	12.3	1.2	40.1	32.8	27.5	23.4	13.4	53
U	15.1	19.2	11.9	51.7	29.6	13.5	18.6	19.1	8.2	8.6	10.9	14.7
La	201	190	264	1020	766	642	226	220	59.8	50.4	89.3	159
Ce	184	155	246	968	714	534	416	400	126	108	155	304
Pr	112	87.5	144	560	418	312	40.9	38.1	14.8	12.7	15	32.8
Nd	40.0	20.0	42.0	152	122	90	132	121	56.7	48.9	47.5	123
Sm	1.43	1.10	2.34	6.57	6.44	2.84	18.5	16.2	10.6	9.2	6.1	21.8
Eu	0.50	0.50	0.28	1.45	1.3	0.58	3.7	3.23	2.03	1.77	1.3	4.17
Gd	n.d.	1.98	1.46	0.30	n.d.	1.06	10.9	9.2	7.3	6.1	3.6	14.5
Tb	n.d.	0.08	0.05	0.29	0.3	0.07	1.3	1	0.9	0.7	0.4	1.7
Dy	n.d.	0.12	0.08	1.73	n.d.	0.45	5.6	4.5	4.1	3.3	1.9	7.7
Ho	n.d.	0.02	0.02	0.33	n.d.	0.09	0.9	0.8	0.6	0.5	0.3	1.2
Er	n.d.	0.10	0.07	0.85	n.d.	0.22	2.5	2	1.6	1.3	0.8	3.1
Tm	n.d.	0.01	0.01	0.11	n.d.	0.03	0.3	0.25	0.2	0.16	0.11	0.37
Yb	n.d.	0.07	0.05	0.65	n.d.	0.18	1.6	1.4	1.2	0.9	0.7	2.2
Lu	n.d.	0.01	0.01	0.10	n.d.	0.03	0.22	0.18	0.16	0.14	0.1	0.31

Note: (1) = Fluor Calcio-carbonatite; (2) = Fluor ore; (3) = Ca-carbonatite; (4) = Carbonatitic leucitite; n.d. = not determined.

calciocarbonatite. The Ficoreto rocks show almost parallel REE patterns, with progressive enrichment passing from tuffisite to dyke rock (Fig. 8d). A comparison among tuffisites from Forcinella, Ficoreto and Polino shows a very similar general pattern at about two orders of magnitude, compared to associated limestone country-rock xenoliths (Fig. 8e). The relative differences are a deeper Zr-Hf negative anomaly and higher positive spike of Sr at Ficoreto. Forcinella tuffisite has higher Cs and Rb. At Ficoreto, the calciocarbonatite breccia dyke has La/Yb at

a value of 105, carbonatite tuffisite at 60 and a hydrothermal deposit at 40 with a slightly negative Eu and positive Gd with La/Yb ratios of 53, 51 and 112 units, respectively (Fig. 7f). Regionally associated limestone xenoliths have a much lower content of REE and low LREE (La_{CN} = 10 pm, with low La/Yb_{CN} = 18) (Rosatelli et al., 2010). Ficoreto tuffisites have a crossover at Nb level with the Forcinella and Polino tuffisites.

Table 2

Seventeen new whole rock analyses of silicate rocks (leucitites and syenites) associated with carbonatites of Table 1. Symbols as in Table 1.

# analyses	MF1701	MF1702	FIC06*	PIA12*	PIA14	RRE02	RRE11	RRE05	RRE07	VEJ27	VEJ3B	VEJ3C	VEJ3D	PIA13	FIC01	PIA01	PIA08
locality**	Forcinella	Forcinella	Ficoreto	Pianciano	Pianciano	RR_FIC	RR_FIC	RR_PIA	RR_PIA	IUP_VUT	IUP_VUT	IUP_VUT	IUP_VUT	Pianciano	Ficoreto	Pianciano	Pianciano
rock-type***	(5)	(5)	(5)	(5)	(5)	(6)	(6)	(6)	(6)	(6)	(6)	(6)	(6)	(7)	(8)	(9)	(9)
litho-facies	lava	lava	scoria	lava	lava	sub. ejecta	sub. ejecta	sub. ejecta	sub. ejecta	sub. ejecta	sub. ejecta	sub. ejecta	sub. ejecta	lava	tuff	tuff	tuff
SiO2 (wt%)	45.17	48.43	46.4	48.3	49.84	52.7	55.9	57.7	56.2	54.9	58.4	57.3	57.1	53.67	49.2	43.32	46.3
TiO2	0.842	0.775	0.73	0.83	0.739	0.873	0.48	0.22	0.18	0.27	0.62	0.23	0.12	0.838	0.73	0.82	0.73
Al2O3	16.2	14.65	12.7	17.2	17.35	15.5	19.8	20.4	20.6	19.5	19.3	20.6	22.1	17.15	16.1	19.49	18.2
Fe2O3	5.15	2.72	5.68	3.60	4.08	2.31	2.14	1.20	1.01	1.90	0.87	1.51	1.11	5.17	6.80	6.03	6.23
FeO	3.3	5.0	1.80	4.50	3.4	4.5	1.80	1.30	1.10	1.10	1.50	1.10	0.80	2	0.20	1.5	0.80
MnO	0.155	0.147	0.13	0.16	0.163	0.14	0.11	0.18	0.15	0.10	0.08	0.19	0.10	0.141	0.13	0.13	0.15
MgO	5.54	6.41	5.69	3.71	3.48	4.42	0.45	0.19	0.12	0.70	0.63	0.33	0.16	2.32	4.00	3.27	1.71
CaO	12.51	12.8	13.6	9.44	9.28	7.26	3.98	2.46	3.24	4.04	2.19	1.85	0.74	6.13	7.30	7.71	3.62
Na2O	1.54	1.22	0.59	1.60	1.83	1.57	3.07	4.40	4.57	4.49	3.20	5.70	7.56	1.86	2.09	0.68	0.69
K2O	7.29	5.87	7.51	8.13	8.54	8.27	10.2	10.1	10.5	8.23	9.94	8.06	7.56	7.12	5.01	1.74	2.51
P2O5	0.55	0.42	0.64	0.52	0.41	0.45	0.07	0.05	0.03	0.16	0.13	0.07	0.04	0.54	0.42	0.43	0.39
CO2	0.01	0.03	1.50	0.02	0.03	0.04	0.02	0.03	0.06	0.17	0.04	0.04	0.04	0.02	0.22	1.16	1.60
S	n.d.	n.d.	n.d.	n.d.	n.d.	0.11	0.14	0.19	1.34	n.d.	n.d.	n.d.	n.d.	n.d.	0.04	0.03	0.11
F	n.d.	n.d.	n.d.	n.d.	n.d.	0.22	0.09	0.11	0.02	n.d.	n.d.	n.d.	n.d.	n.d.	0.11	0.31	0.17
LOI	0.18	0.11	2.41	1.04	0.45	1.44	1.75	1.49	1.19	4.52	1.58	1.77	1.40	1.20	7.82	11.84	11.9
SrO	0.19	0.18	0.21	0.27	0.24	0.22	0.48	0.19	0.19	0.28	0.44	0.11	0.06	0.16	0.17	0.16	0.39
BaO	0.16	0.13	0.19	0.21	0.16	0.21	0.24	0.04	0.11	0.17	0.29	0.05	0.04	0.19	0.17	0.75	4.24
Total	**98.8**	**98.9**	**99.8**	**99.6**	**100.0**	**100.2**	**100.7**	**100.3**	**100.5**	**100.5**	**99.2**	**98.9**	**98.9**	**98.5**	**100.6**	**99.4**	**99.6**
O=F	—	—	—	—	—	0.09	0.04	0.05	0.01	—	—	—	—	—	0.05	0.13	0.07
Total	**98.8**	**98.9**	**99.8**	**99.6**	**100.0**	**100.1**	**100.7**	**100.2**	**100.5**	**100.5**	**99.2**	**98.9**	**98.9**	**98.5**	**100.5**	**99.2**	**99.6**
Mg#	0.75	0.70	84.9	59.5	0.65	0.64	0.31	0.21	0.16	0.53	0.43	0.35	0.26	0.67	0.97	0.80	0.79
V (ppm)	270	240	251	255	239	207	150	67	74	58	67	46	18	183	207	192	179
Sc	15	26	29	14	15	21	2	< 1	< 1	2	2	< 1	< 1	14	19	16.9	13.2
Cr	40	160	100	50	40	120	< 20	< 20	< 20	30	< 20	< 20	< 20	30	100	107	57.6
Co	32	30	33	25	23	22	4	1	1	4	5	2	1	19	22	22.3	25.9
Ni	60	70	80	30	30	60	< 20	< 20	< 20	< 20	< 20	< 20	< 20	< 20	60	48	28
Cu	110	60	110	80	70	30	< 10	< 10	< 10	10	< 10	< 10	< 10	30	80	93	79
Zn	80	80	70	80	80	90	60	120	110	70	50	80	60	90	80	204	148
As	11	9	11	< 5	< 5	14	19	8	14	33	11	15	16	< 5	19	< 1	< 1
Rb	446	374	527	446	470	386	363	165	188	252	233	276	363	401	452	210	170
Sr	1642	1498	1768	2289	2013	1846	4071	1581	1581	2374	3760	916	470	1320	1472	1364	3315
Y	29	30	30	34	33	28	57	8	6	15	55	31	5	28	30	23	36
Zr	312	299	359	364	344	413	562	436	491	332	410	724	1040	364	306	349	400
Nb	13	14	16	25	20	34	36	29	29	139	182	176	255	24	18	35	58
Cs	39.1	24.5	47	35	41	14.1	13.4	2.1	2.4	8.3	12	19.8	17	21.5	48.1	65.4	48.5
Ba	1389	1127	1679	1857	1473	1850	2114	358	1003	1516	2576	458	323	1673	1515	6757	37950
Hf	5.9	5.9	8.2	8.1	7.7	10.7	10.1	6.6	6.6	4.6	6.5	10.3	11.1	9.3	7.4	10.1	11
Ta	0.7	0.8	0.7	1.1	0.9	1.9	2.3	1.1	1	5.3	14.7	4.7	8	1.4	1	< 0.3	< 0.3
Pb	78	55	55	102	97	100	152	171	99	123	137	77	51	87	84	1050	663
W	5	5	6	6	5	7	9	5	17	3	< 1	< 1	< 1	5	10	131	70
Th	45.5	41.1	63.6	62	56.5	47.5	149	109	94.4	78.7	366	131	85.2	57.9	49.1	68.6	56.9
U	9.5	9.3	12.3	12.3	10.7	8.7	29.8	27.2	26.5	37.2	40.7	46	77.9	12.6	9.5	2.6	32.2
La	96.2	92.1	134	139	128	121	168	240	164	213	410	489	117	122	130	136	559
Ce	200	189	285	269	254	245	325	399	296	308	707	612	167	227	246	217	554
Pr	22.8	21.9	32.6	30.2	28.3	27.8	35.4	35.6	26.9	26.2	67.1	38.5	11.4	26.4	27	n.d.	n.d.
Nd	90.7	84.7	128	109	105	102	123	89.5	68.8	71.5	204	82.2	25.4	96.9	97.8	72	124
Sm	16.9	16	24.1	19.4	18.6	17.9	22	7.6	5.8	8.3	29.6	8	2.5	16.9	16.8	15.9	15.9
Eu	3.39	3.2	4.64	3.88	3.71	3.36	4.48	1.12	0.8	1.84	6.56	1.75	0.49	3.43	3.18	2.3	3.2
Gd	11.2	11.1	16.4	13	12.8	11.8	15.3	3	2	4.9	18.7	5	1.3	11.5	11	n.d.	n.d.
Tb	1.4	1.3	2.1	1.6	1.6	1.4	2.1	0.3	0.2	0.6	2.4	0.8	0.2	1.4	1.4	1.3	1.3
Dy	6.4	6.5	9.1	7.6	7.4	6.7	10.6	1.3	0.9	3	12.1	4.7	0.9	6.7	6.6	n.d.	n.d.

6

Table 2 (continued)

	MF1701	MF1702	FIC06*	PIA12*	PIA14	RRE02	RRE11	RRE05	RRE07	VEJ27	VEJ3B	VEJ3C	VEJ3D	PIA13	FIC01	PIA01	PIA08
# analyses																	
locality**	Forcinella	Forcinella	Ficoreto	Pianciano	Pianciano	RR_FIC	RR_FIC	RR_PIA	RR_PIA	IUP_VUT	IUP_VUT	IUP_VUT	IUP_VUT	Pianciano	Ficoreto	Pianciano	Pianciano
rock-type***	(5)	(5)	(5)	(5)	(5)	(6)	(6)	(6)	(6)	(6)	(6)	(6)	(6)	(7)	(8)	(9)	(9)
litho-facies	lava	lava	scoria	lava	lava	sub. ejecta	sub. ejecta	sub. ejecta	sub. ejecta	sub. ejecta	sub. ejecta	sub. ejecta	sub. ejecta	lava	tuff	tuff	tuff
Ho	1.1	1.1	1.5	1.3	1.2	1.1	1.9	0.2	0.2	0.5	2	1	0.2	1.1	1.1	n.d.	n.d.
Er	2.8	3	3.6	3.2	3.2	2.8	5.2	0.6	0.5	1.4	5.1	3.1	0.4	3	2.9	n.d.	n.d.
Tm	0.38	0.4	0.44	0.45	0.46	0.36	0.71	0.09	0.07	0.2	0.64	0.54	0.08	0.4	0.39	n.d.	n.d.
Yb	2.3	2.4	2.5	2.6	2.7	2.1	4.6	0.6	0.4	1.2	3.4	3.6	0.5	2.4	2.3	1.84	2.43
Lu	0.34	0.37	0.36	0.37	0.36	0.3	0.68	0.09	0.06	0.17	0.4	0.55	0.06	0.36	0.35	0.15	0.51

Note: * = K/Ar geochronology test; ** = RR_FIC = Roman region foid syenite from Ficoreto; RR_PIA = Roman region foid syenite from Pianciano; IUP_VUT = Vulture volcano foid syenite from Pianciano; IUP_VUT = Vulture volcano foid syenite; *** (5) = Leucitite; (6) = Alkali feldspar syenite; (7) = Trachite; (8) = epithermal deposits; (9) = altered leucitite tuff; sub. ejecta = subvolcanic ejecta; n.d. = not determined.

3.1. Isotope geochemistry

RR carbonatites have very radiogenic $^{87}Sr/^{86}Sr$ (0.709–0.712) as well as un-radiogenic $^{143}Nd/^{144}Nd$ isotopic ratios (ε_{Nd} −8.5 to −14), which are in isotopic equilibrium with the associated mafic alkaline silicate rocks and exceed Enriched Mantle 2 end-member (EM2) values in radiogenic Sr (Fig. 9a, Table 3b). IUP rocks partially overlap the RR data in the covariation Sr/Nd diagram, while Forcinella lavas plot in between (Fig. 9a). Vulture has much lower values but shows some possible EM2 enrichment. Italian ultra-alkaline rocks are on a trend-line passing through Italian lamproites and lamprophyres (Vichi et al., 2005), and an extremely enriched mantle end-member, named ITEM (Bell et al., 2013). Notably, mantle-derived Polino phlogopite plots along the trend-line near the ITEM. Italian Triassic-Jurassic limestones and dolostones (Di Battistini et al., 2001; Rosatelli et al., 2010) are located between the Bulk Silicate Earth - EM1 and EM2 triangle and RR rocks. In general, previous authors noticed that the isotopic ratio decreases from northern to southern Italy on a regional scale (Bell et al., 2013).

Ten new $\delta^{13}C$ and $\delta^{18}O$ ratio determinations of RR and other Italian carbonatites can be added to the previous literature (Fig. 9b, Table 3b). Stable isotopes were determined at the Mass Spectrometry Laboratory of the IGAG-CNR in Rome, using a Finnigan Mat 252 mass spectrometer and a Finnigan Kiel II device for the extraction of CO_2 from the $CaCO_3$. Vulture carbonatites plot very close to the mantle box values (PIC). All the extrusive Italian carbonatites show a general variation trend with $\delta^{18}O$ positive and $\delta^{13}C$ negative shifts (Fig. 9b). In the Pianciano carbonates, $\delta^{13}C$ varies from −3.87‰ to −4.47‰, and $\delta^{18}O$ from 14.64‰ to 16.20‰, respectively. Carbonates at Ficoreto show large variations of both C and O isotopic ratios. These data cluster in two distinct areas: the dyke rock (FIC04, Table 1) has $\delta^{13}C$ (vs PDB) −3.81‰ and $\delta^{18}O$ (vs SMOW) 18.05‰, while tuffisite rock (FIC05, Table 1) has $\delta^{13}C$ ranging from −11.31 to 12.01‰, and $\delta^{18}O$ ranging from 23.25 to 24.25‰. In particular, Ficoreto tuffisites match the values of Polino tuffisite (Fig. 9b), while massive Polino calciocarbonatite has less extreme values (Fig. 9a). Masi and Turi (1971, 1976) report that Ficoreto dyke rocks average $\delta^{13}C$ = −2.31‰ and $\delta^{18}O$ = 17.13‰ (close to the values of sample FIC04) and report less extreme values for the fluor ore deposits of Corso Francia in Rome city. Forcinella has $\delta^{18}O$ 20.95‰ and $\delta^{13}C$ −7.11% values, very close to Cupaello carbonatite tuff (Stoppa and Cundari, 1995). San Venanzo carbonatitic tuffisite shows more extreme values for $\delta^{13}C$ and $\delta^{18}O$ of −14.0 and 23.0‰, respectively (Table 3b). Italian limestones have positive $\delta^{13}C$ > 2‰ and $\delta^{18}O$ > 28‰ (Fig. 9b).

4. Discussion

The vast majority of authors agree about a mantle origin of carbonatites according with experimental petrology. The geological evidence indicates that Italian extrusive carbonatites frequently formed fluidised breccias carrying mantle nodules in diatremes (tuffisite). The Italian carbonatites also show a wide range of compositions (primitive silico-carbonatites with mantle nodules, calciocarbonatites and fluor-calcio-carbonatites), which are particularly suitable, in our opinion, for investigating a complex carbonatite system. Popular differentiation processes, such as immiscibility and crystal fractionation, are considered to be crucial (Martin et al., 2012). Plastically deformed carbonate globules in the groundmass of the melilite leucitite lapilli, found in the tuffisite, together with carbonatitic lapilli, are both textural evidence for the magmatic development of immiscibility. Petrographic studies indicate that, after carbonatite immiscibility, essential mineral phases precipitated between 650 and 900 °C, based on the paragenetic relationship of calcite, fluorite and periclase (Treiman and Essene, 1984; Kokh et al., 2015). The formation of monticellite and garnet at the contacts between silicates and carbonates are convincing signs of magmatic reactions at shallow crustal pressures. Sulphate minerals and

Table 3a

Two new K-Ar dating performed at Activation Laboratories (www.actlabs.com), analyst Mahadi Ghobadi.

Locality	Rock type	Sample	K, % ± σ	^{40}Ar rad, (ng/g)	% ^{40}Ar air	Age, Ma	Error 2σ
Ficoreto	leucitite	FIC06	5.82 ± 0.06	0.0864 ± 0.0017	57.0	0.214	0.010
Pianciano	leucitite	PIA12	6.51 ± 0.07	0.0910 ± 0.005	83.7	0.200	0.020

REE-fluorcarbonates precipitated as a very fine-grained matrix as cooling proceeded. It is necessary to confirm all these puzzling details with multiple convergent lines of investigation. In addition, this paper serves to focus attention on carbothermal processes, with a high CO_2 partial pressure, equivalent to the pegmatitic stage, and the hydrothermal stage because many ore-deposits are associated with late stage carbonatites (Mitchell, 2005).

Our model focuses on the relationship of the fluor ore with fluor-calciocarbonatite and alkaline rocks. This link has been seen in several carbonatite complexes associated with fluor ore. Italian primitive carbonatites are in general small volume whereas fluor-calciocarbonatites (i.e. Pianciano) are large volume. A composition very similar to Pianciano rocks is from REE-rich Lizhuang ore, having calcite (76%), fluorite (14%), barite (3%), mica (3%), quartz (2%) and bastnäsite (2%), and even La/Y (~69) and Pb content (1375 ppm) (Liu and Hou, 2017).

4.1. Geochemistry

Italian carbonatites are similar to worldwide extrusive carbonatites, having an enrichment in LREE and Sr over HREE and $HFSE^{4+5+}$, which appears to be a characteristic of mantle carbonatites according to Jones et al. (1996, 2013), Nelson et al. (1988) and Zaccarini et al. (2004). Subtypes of REE-carbonatites with > 1 wt% REE_2O_3 (Jones et al., 2013) are very rare among extrusive carbonatites, which in general have < 5000 ppm of LREE. LREE contents in these rocks are directly related to fluorine content and this may apply to several Italian carbonatite localities.

Cr, Ni, Cs, V and Pb are unusually high in Italian carbonatites. The high Cr-Ni content in Italian carbonatites and associated rocks correlates to the amount of Cr-phlogopite, Cr-diopside, forsterite and chromite mantle xenocrysts. According to Bell and Kjarsgaard (2006), the presence of mantle debris in Italian carbonatites "is a testament to the rapid ascent of the carbonatitic magmas". High caesium is hitherto rare in carbonatites. Among 256 worldwide carbonatites with Cs above the detection limit (generally 0.2–0.5 ppm by INAA, FUS-MS respectively)

and an average of 3.6 ppm, only 46 samples have a Cs content above the average and up to 55 ppm. Two thirds of the deposits are extrusive. Carbonatites in West Qinling (China), Western Baikal area (Russia), Samalpatty (India) and Oldoinyo Lengai (Tanzania) have a similar specific geochemistry (Savelyeva et al., 2016; Zaitsev and Keller, 2006). High Cs is a significantly distinctive feature of these extrusive carbonatites and is poorly related to Rb in Italian carbonatites. A discrete Cs-bearing mineral of the vanadate group might be expected to occur in the Pianciano carbonatite and fluor ore. V is a characterising element of carbonatites and may reach > 1000 ppm in Glenover-Namibia, Lizhuang-China and Amba Dongar-India carbonatites (e.g. Viladkar et al., 2019), but is usually < 500 ppm. Italian carbonatites form two groups: primitive calciocarbonatites with relatively low V and REE, and evolved fluor-calciocarbonatites with high V and REE.

We found that $LFSE^{2+}$ and $HFSE^{2+3+}$ (Sr, Ba, REE, V) are partitioned into the carbonate phases and $HFSE^{4+5+}$ into a silicate phase. Italian carbonatites do not neatly conform to established mantle 'immobile' ratios, which should be quite insensitive to crystal settling and reflect the mantle source condition and composition when the parental melt was generated (Pearce, 2008). In Fig. 7, rocks outside the mantle array are potential scavengers of specific HFSE. We explain this geochemical peculiarity as because of immiscibility processes. In fact, $HFSE^{4+5+}$ have different fractionation coefficients for silicates and carbonates (Chakhmouradian, 2006). Shifting or decoupling of co-magmatic carbonatite compositions in 'immobile' ratio diagrams is a fingerprint for the silicate-carbonatite immiscibility process (Brod et al., 2013). Thus, we favour immiscibility rather than crystal fractionation in this case, owing to the rapid propagation of the magma towards the earth surface (10 m s^{-1}, estimated by mantle nodules mass). A one order of magnitude of $HFSE^{4+5+}$ over HREE fractionation is particularly evident at Ficoreto, where facies range from pure calciocarbonatite to mixed carbonatite and carbonatitic melilite leucitite (Fig. 7a, c). It is characteristic to find that carbonatite has a higher LREE/HREE ratio in comparison with conjugate silicate melts (Stoppa et al., 2005). The LREE/HREE ratio in carbonatites is controlled by both major and minor phases and vapour phase fractionation (Jones et al., 2013). In

Table 3b

Thirteen radiogenic and stable isotopes new analyses of Italian carbonatites and reference compositions obtained at Lab IGAG-CNR Montelibretti Italy, analyst Mauro Brilli (stable isotopes) and IGAG-CNR *Roma Sapienza*, analyst Francesca Castorina (Sr-Nd isotopes).

Locality	Rock type	Sample	$^{87}Sr/^{86}Sr$ ± 2se	$^{143}Nd/^{144}Nd$ ± 2se
Ficoreto	hydrothermal deposit	FIC01 cc[(b)]	0.709819 ± (10)	0.512096 ± (6)
Ficoreto	Ca-carbonatite (dyke)	FIC04 cc	0.709017 ± (4)	0.512090 ± (7)
Ficoreto	Ca-carbonatite	FIC05b cc	0.709842 ± (9)	0.512093 ± (10)
Forcinella	carbonatitic leucitite	MF1703	0.709810 ± (10)	0.512109 ± (8)
Pianciano	fluor ore	PIA02 cc	0.709620 ± (9)	0.512136 ± (13)
Pianciano	fluor ore	PIA03 cc	0.709639 ± (8)	0.512141 ± (9)
Pianciano	fluor Ca-carbonatite	PIA06 cc	0.709617 ± (8)	0.512115 ± (8)

Note: 2se = standard error; cc = carbonate fraction.

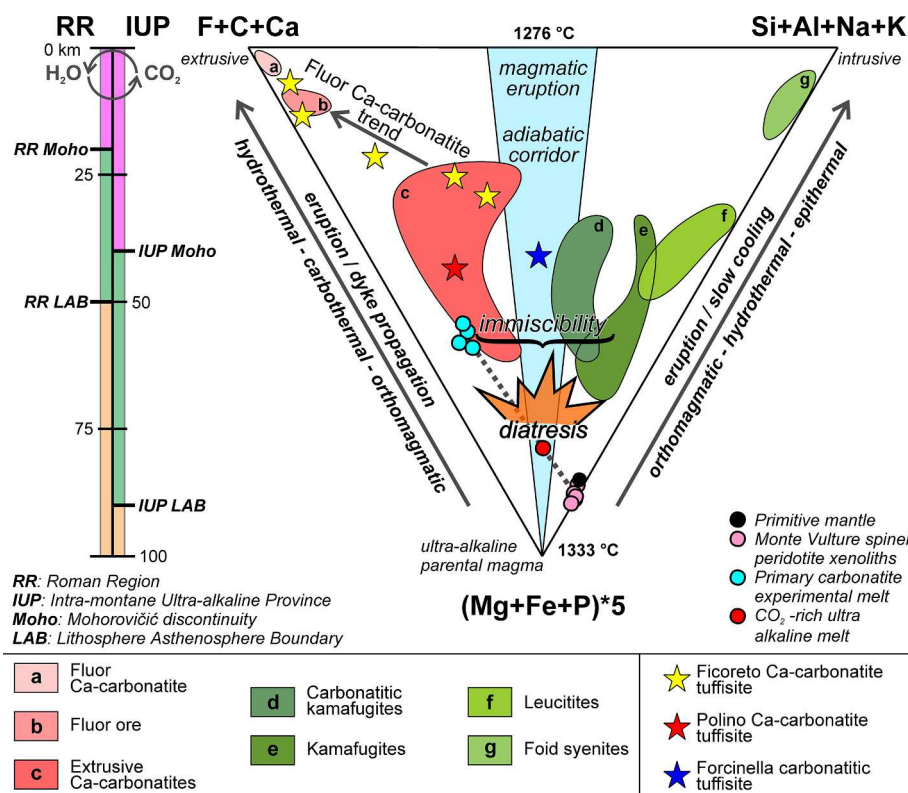| Locality	Rock type	Sample	$\delta^{13}C$ (V-PDB)	$\delta^{18}O$ (V-SMOW)
Ficoreto	Ca-carbonatite (dyke)	FIC04 cc	−3.81	18.05
Ficoreto	Ca-carbonatite	FIC05b cc #3 avg.	−11.96	24.10
Ficoreto	Ca-carbonatite	FIC05d cc	−11.31	23.25
Forcinella	carbonatitic leucitite	MF1703	−7.11	20.95
Pianciano	fluor Ca-carbonatite	PIA05 cc #2 avg.	−4.36	14.92
Pianciano	fluor Ca-carbonatite	PIA06 cc #2 avg.	−3.98	13.82

Fig. 4. Ternary diagram illustrating different ultra-alkaline rock-types and petrogenetic system processes, parental melt and derivative rock-types based on PETROS-3 software outputs (Petrov and Moshkin, 2015). Data are from supplementary data 1 and 2. New whole rock data are in Tables 1 and 2. Primary melt at the lithosphere/asthenosphere boundary lies on a line linking mantle compositions (Dalton and Wood, 1993; Downes et al., 2002; Lyubetskaya and Korenaga, 2007) and experimental carbonatitic melts (Sweeney, 1994 and references therein), crossed by the adiabatic path of ultra-alkaline melts. Above this line, there is the diatresis point and violent CO_2 exsolution after Bailey (1985). Forcinella tuffisite (blue star) represents the ideal candidate to demonstrate the tuffisitisation process, being exactly on the eruptive path. After immiscibility, the carbonatite system diverges from mafic silicate derivatives. The depth of the MOHO and Lithosphere-Asthenosphere Boundary (LAB) are from Lavecchia et al. (2002, 2006). The depth of mantle metasomatism, diatresis and immiscibility are after Bailey (1985). Kamafugite temperatures at 1 bar are from Cundari and Ferguson (1991).

Italian REE-rich carbonatites, Y concentrates in fluorite, whereas the amount of HREEs drops dramatically (Fig. 7d). The LREE/HREE ratio marks an increase of carbonatitic liquid differentiation. In fact, the REE patterns of Italian co-magmatic carbonatites cross over when more evolved facies, having higher LREE/HREE ratios, are compared with less evolved facies (Fig. 8). As a whole, Italian carbonatites conform to the general geochemical features of worldwide extrusive carbonatites without deviation; some specific signatures have been seen in other carbonatites, but these do not represent a petrological challenge and can be explained by trace element fractionation between the carbonate and silicate components.

4.2. Isotopes

Italian ultra-alkaline rocks have high radiogenic $^{87}Sr/^{86}Sr$ ratios and un-radiogenic $^{143}Nd/^{144}Nd$ isotope ratios. Similar Sr isotope-enriched carbonatites, although unusual, have been identified in the Amba Dongar carbonatite, India (Deans and Powell, 1968; Simonetti et al., 1995) as well as at Phalaborwa, South Africa (Eriksson, 1989), Walloway, Australia, Jacupiranga, Brazil (Nelson et al., 1988), southwest Transbaikalia (Doroshkevich et al., 2008), Laiwa-Zibu, Fangcheng China (Ying et al., 2004) and Mianning-Dechang (Hou et al., 2015; Liu and Hou, 2017). In all cases, they are associated with alkaline silicate magmas that have equally elevated initial $^{87}Sr/^{86}Sr$ ratios. Italian carbonatites are associated with mantle-derived kamafugites, so their high Sr isotope ratios are interpreted as the result of an enriched mantle source (Castorina et al., 2000; Rosatelli et al., 2007). Mantle nodules from IUP indicate a carbonate-bearing, phlogopite–clinopyroxene source with highly radiogenic $^{87}Sr/^{86}Sr$ and un-radiogenic $^{143}Nd/^{144}Nd$ (Di Battistini et al., 2001; Rosatelli et al., 2007; Castorina et al., 2000). Notably, both the IUP carbonatites and their associated alkaline mafic silicate rocks preserve isotopic and chemical equilibrium. This

Fig. 5. Diagrams a) and b) plot geochemical data grouped by principal component defined by rank statistics La + Ce + V + Ba/100 and Rb + Zr + Nb vs. F + C + Ca and Si + Al + Na + K factors, respectively. Data are from supplementary data 1 and 2. Symbols as in Fig. 4.
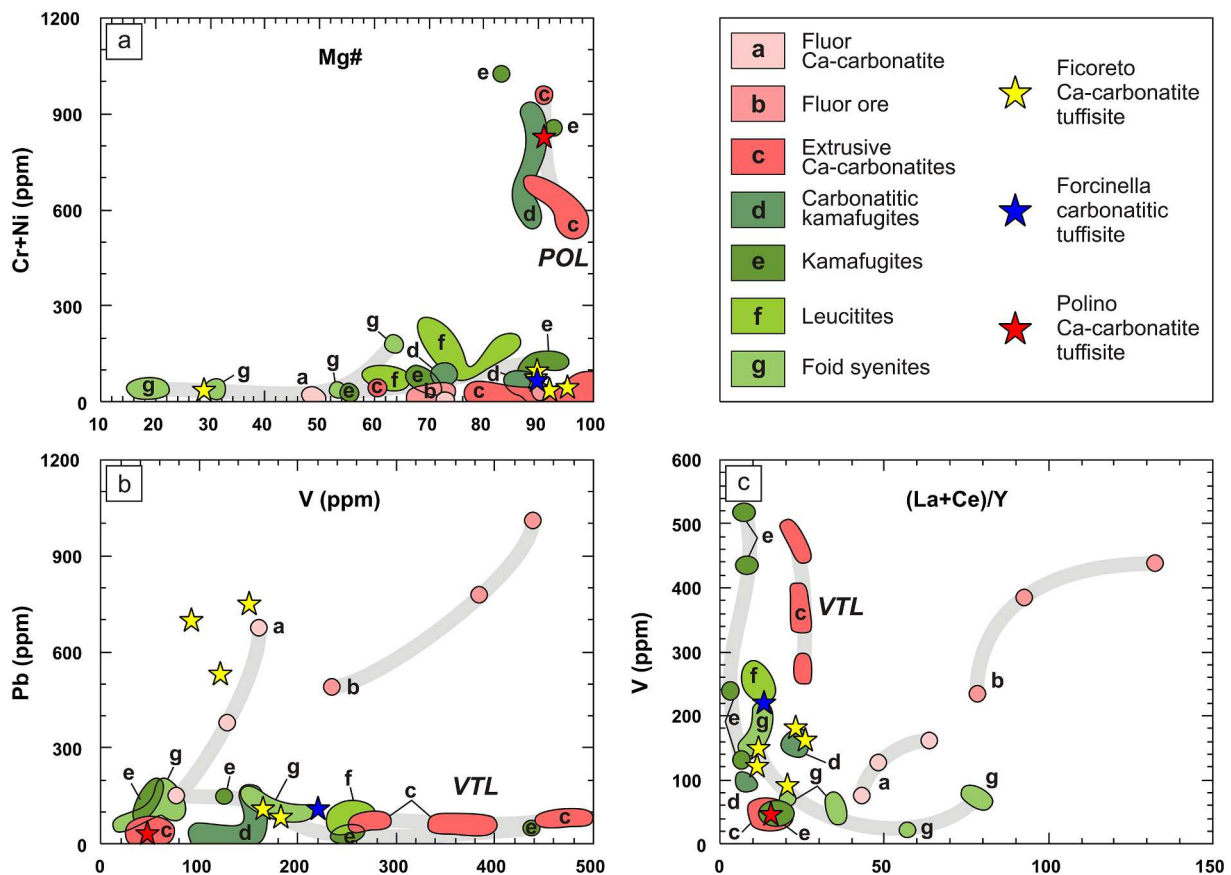
Fig. 6. Miscellaneous geochemical characteristics of Italian ultra-alkaline rocks (data from Tables 1 and 2 and literature cited in the text. a) High Cr + Ni when associated with high Mg# indicates an abundance of mantle debris in Italian ultra-alkaline rocks, debris are inherited during immiscibility; b) A peculiar feature shared with a few other carbonatites (see the text) is the abundance of Pb and V; c) Italian fluor-calciocarbonatites concentrate specific elements (Pb and V) with an increase of the La/Y ratio. Acronyms POL = Polino, VTL = Vallone Toppo del Lupo.

coherence is only compatible with a closed system and magmatic differentiation, with the carbonate fraction derived by either fractional crystallisation or liquid immiscibility from a common parental magma (Stoppa et al., 2005). The isotopic signature is distinctive and may be associated with the Nd-Sr-Pb mantle end-member called 'Italian Enriched Mantle' (ITEM) (Bell et al., 2013). Both the RR and the IUP share isotopic characteristics for Nd, Pb and Sr, which trend towards this ITEM mantle end-member (Fig. 9a).

A common feature of the stable isotopes in carbonates associated with extrusive carbonatites is their linear co-variation with decoupled $\delta^{18}O$ positive and $\delta^{13}C$ negative trends (Fig. 9b). This trend is characteristic of global carbonates in carbonatites, kimberlites and lamprophyres, and is widely interpreted as being produced by a magmatic process (Deines, 1989; Demény and Harangi, 1996). Previous authors interpreted the variation observed in the RR carbonatites and fluor ore as being the result of precipitation of calcite from circulating superficial waters enriched in organic C or from carbonated thermal waters (Masi and Turi, 1971, 1976). However, the high temperature mineralogical assemblage of the RR carbonatites allows for a different explanation. Demény et al. (1994) suggested that the negative $\delta^{13}C$ shift derives from solid-vapour fractionation during exsolution of CO_2 dissolved in the parental magma. The degree of CO_2 escape from the parental magma would determine the extent of ^{13}C depletion in the residue and thus the $\delta^{13}C$ values of carbonates precipitated from such an evolved fluid, as was experimentally determined (e.g. Mattey et al., 1990). There are assumptions of kinetics, and mass volume connectivity by diffusion, which are implied. These conditions would probably generate heterogeneity, unless subsequent turbulent magma mixing was

involved, but could also lead to immiscibility in the liquids and in the vapour phases (Lowenstern, 2001).

The fluor ore has increasingly positive $\delta^{18}O$ and negative $\delta^{13}C$ isotopic ratios. $\delta^{13}C$ is very negative; it is lower than those typical for primary mantle carbonatites, reaching -13.5. However, $\delta^{18}O$ is very positive and much higher than Primary Igneous Carbonate (PIC). Santos and Clayton (1995) concluded that the largest contributor to elevated $\delta^{18}O$ values in carbonatites is the release of one or more phases of H_2O–CO_2 fluids from degassing magma that was allowed to equilibrate with the carbonatite. Textural indications of rapid carbonate quenching, together with high-T minerals, for example in the Ficoreto and Polino calciocarbonatites, and the presence of Sr, REE and P in the groundmass, rule out secondary low-temperature hydrothermal alteration/precipitation of calcite. These rocks are fresh, unaltered, and their isotopic composition can be attributed to CO_2 degassing during crystallisation and fractionation between calcite and CO_2-H_2O fluid under evolving XCO_2 (Demény and Harangi, 1996). C and O variations are equally large among different outcrops or in a single outcrop, ruling out local fractionation processes. This suggests that the calcite matrix is a quenched carbonatite liquid, which underwent CO_2 degassing at T > 500 °C, when the CO_2 gas was isotopically heavier than the associated calcite (Chacko et al., 1991).

Some geochemical peculiarities of carbonatites, especially stable isotopes, have often been linked back to low-temperature near-surface meteoric water (supergene) exchange. In our opinion, this phenomenon has a minor importance if we exclude meteoric waters mixing with the hydrothermal system.
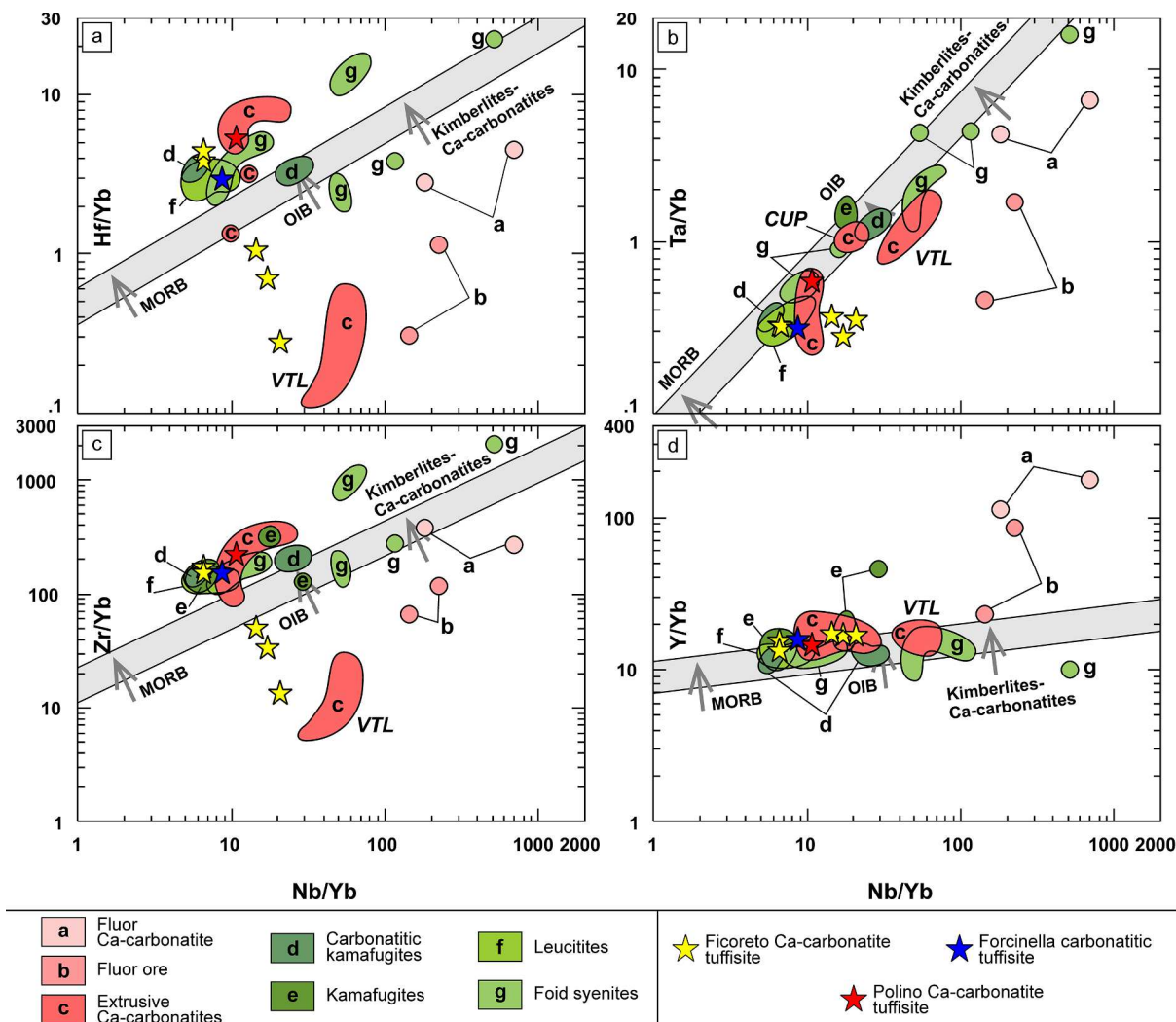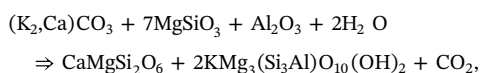
Fig. 7. 'Immobile pairs' diagrams. The mantle array as defined by Pearce (2008 and references therein) is in grey. Arrows indicate the position of worldwide MORB, OIB, kimberlites and calciocarbonatites. Italian ultra-alkaline rocks plot in the range of OIB, extending over the carbonatite-kimberlite plotting area. Compositions that detach from the mantle array have a special ability to fractionate HFSE and REE strongly. Data from Tables 1 and 2 and literature cited in the text. Acronyms CUP = Cupaello, VTL = Vallone Toppo del Lupo.

4.3. Magmagenesis, metasomatism and petrogenesis

Experimental petrology suggests that the formation of primary carbonatite melts (average ~15 wt% MgO and ~21 wt% CaO plus ~8 wt% alkalis) can occur by low degree melting of carbonated peridotite (Sweeney, 1994 and references therein). However, a pure carbonatite, formed in near solidus conditions, is not easily eruptible and, when magma passes through the thermal boundary layer, it probably impacts on the lherzolitic solidus. This event can consume carbonate by metasomatic reactions:

$$CaMg(CO_3)_2 + 4MgSiO_3 \Rightarrow CaMgSi_2O_6 + 2Mg_2SiO_4 + 2CO_2$$

and

$$(K_2,Ca)CO_3 + 7MgSiO_3 + Al_2O_3 + 2H_2O$$
$$\Rightarrow CaMgSi_2O_6 + 2KMg_3(Si_3Al)O_{10}(OH)_2 + CO_2,$$

which could explain phlogopite wehrlite veins found in Italian lherzolite mantle xenoliths (Rosatelli et al., 2007). CO_2 widely degasses from active magmatic systems and moves towards the surface, as evidenced by high CO_2 flow in Italy (Gambardella et al., 2004). To avoid total carbonate consumption by metasomatism, magma has to come up from a deeper and hotter mantle level. This postulates complex mass

transport, flux, and velocity calculation but is rather constrained by carbonate peridotitic solidus and local geotherm (Presnall and Gudfinnsson, 2005). If C-rich magma flows rapidly in a conduit through the lithosphere (diatresis), following an adiabatic geotherm at temperatures above the lherzolite solidus, it may escape solidification and erupt to the surface. Campeny et al. (2014) consider the primary magma to be a batch of silicocarbonatite from a single deep-mantle melting event. In fact, if the subasthenospheric mantle is strongly reducing, a pure carbonatite melt may be unlikely to form (Brooker and Kjarsgaard, 2011). When the pressure is greater than > 40 kbar, the partial melting decreases in the CO_2-bearing lherzolite and CO_2 decreases, whereas SiO_2 increases to form silicocarbonatite, also at low melting temperatures (Gudfinnsson and Presnall, 2005). Italian carbonatites are in equilibrium with alkaline melts and, thus, their parental melt has to be alkaline (Weidendorfer et al., 2017). Experimental petrology supports this observation (Martin et al., 2013). In addition, Vulture carbonatites and IUP rocks preserve the co-crystallisation of nyerereite and calcite in melilite and clinopyroxene inclusions (Stoppa et al., 2009; Panina et al., 2003; Isakova et al., 2017). Testing this model in Fig. 4, the experimental primary carbonatites lie outside the likely eruptive adiabatic decompression path ("corridor") and are different from the notional alkaline silico-magnesiocarbonatite calculated at the intercept of the eruptive adiabat corridor with the line linking the
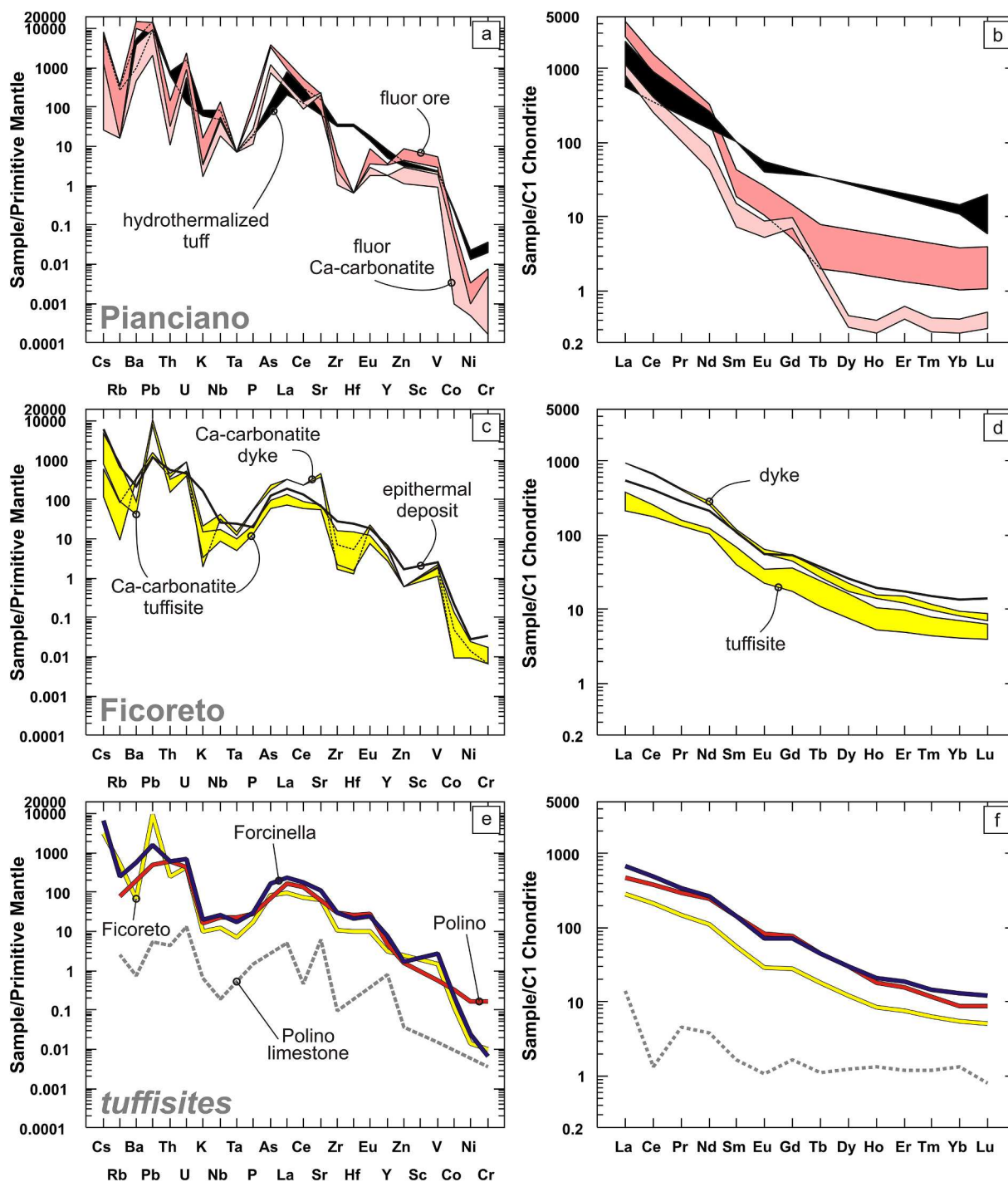
Fig. 8. Multi-element diagrams Tables 1 and 2 and literature cited in the text. a) Primitive-mantle normalised (Sun and McDonough, 1989), LFS and HFSE patterns of Pianciano carbonatites and associated fluor ore and altered tuffs; b) Chondrite normalised REE patterns for Pianciano fluor-calciocarbonatite, fluor ore and altered tuffs; c) Primitive-mantle normalised LFS and HFSE patterns for Ficoreto calciocarbonatite dyke rocks (FIC03, FIC04), calciocarbonatite tuffisite (FIC8a) and hydrothermal deposits (FIC01); d) Chondrite normalised REE patterns for calciocarbonatite dyke rocks (FIC03, FIC04), calciocarbonatite tuffisite (FIC8a) and hydrothermal deposits (FIC01); e) Primitive mantle normalised multi-elements diagram showing Forcinella carbonatitic tuffisite, Ficoreto calciocarbonatite tuffisite and Polino calciocarbonatite tuffisite. Polino limestone country-rock is shown for comparison; f) Chondrite normalised REE pattern for Italian carbonatitic tuffisites from Ficoreto, Forcinella and Polino. Polino limestone country-rock is shown for comparison.

experimental primary carbonatite and mantle composition (Fig. 4). We explain the difference with a deeper source and the physical or virtual content of mantle debris that would be able to react with carbonate liquid. Concerning the mechanism of magma propagation through the lithosphere, there is evidence for a rapid and energetic mechanism to explain the abundance of mantle nodules. Very rapid emplacement is also in accord with the quenching of carbonatite melts, and the

extremely rapid nucleation and crystallisation of carbonate, producing a cryptocrystalline groundmass and micropellets (carbonate droplets). Bailey (1985) constructed the model of diatresis to explain the formation of tuffisite. Diatresis occurs when there are constraints due to the CO_2 solubility limit, magma composition and local geotherms. Violent CO_2 exsolution propels the magmatic convoy to the surface at high speeds. Diatresis produces a fluidised mantle peridotite breccia, which

Fig. 9. a) Conventional Sr and Nd isotope diagram showing the enriched quadrant where the Roman Region and IUP rocks plot. The diagram displays the BSE, EMI and EMII triangle, which represents the usual metasomatised mantle source compositional field, the Italian Triassic and Jurassic dolostones and limestones compositional field (unpublished data courtesy of Bell K.), the Italian lamprophyres trend and Italian Enriched Mantle (ITEM) isotopic end-member of Bell et al. (2013); b) C and O isotopes of Italian carbonatites. Primary Igneous Carbonatite (PIC) represents the mantle composition (Taylor, 1985). The results are expressed in the usual d-notation, where the reference standards are Pee Dee Belemnite (V-PDB) for C and standard mean oceanic water (V-SMOW) for O.

rapidly disaggregates into finer mantle debris, immersed into an emulsion of immiscible carbonatite-silicate melts and leading to the typical tuffisite texture (Lloyd and Stoppa, 2003). We suggest that the reactive surface area, kinetics and size distribution of mantle debris versus liquid during fluidisation (diatremic propagation) has an active, unevaluated role in magma differentiation. Jones et al. (2000) used a range of geothermometers/barometers for Vulture mantle nodules, which gave an indication of detachment from the mantle at a maximum of 22 kbar, a value that is in accord with the diatresis model.

The experimental study by Martin et al. (2012) demonstrated that Italian carbonatite and kamafugite melts are immiscible at 17 kbar and 1220 °C, above the diatresis limit. Based on textural and experimental evidence, and rock geochemistry, we assume that diatresis and immiscibility were the dominant magmatic phenomena at mantle depth.

In Figs. 4 and 10, rock compositions are ideally associated with different physical processes. Magma can erupt along a diatremic/adiabatic corridor as a mechanical mixture of the carbonate and silicate component or as the carbonatite and silicate mafic alkaline systems

diverge and evolve up to their minimum 'solidus' and later, fluid-dominated, stages. The lower corner of the diagram in Fig. 3 represents conditions at the lithosphere-asthenosphere boundary (LAB) depth and high-T liquidus, CO_2-rich alkaline silicate melt (Lavecchia et al., 2002; Isakova et al., 2019). The F-C-Ca corner represents the "endstop" of fluor-calciocarbonatites and so-called "residua" deposited under carbothermal-hydrothermal conditions (Mitchell, 2005). The Si-Al-Na + K corner represents evolved orthomagmatic foid syenite or trachyte near the phonolitic minimum (Carmichael, 1964). Carbonatite, fluor-calciocarbonatite and fluor ore deposits trend on the left side up to the F-C-Ca corner. Notably, Ficoreto carbonatite dykes cover a range of compositions, from IUP carbonatites to RR extrusive fluor-calciocarbonatites. Forcinella carbonatitic tuffisite is an ideal composition representing eruptible silicocarbonatite in this model. The main textural and mineralogical evolution is depicted in Fig. 10.

Gupta and Yagi (1980) and Velde and Yoder (1976) described a lot of silicate-carbonate system reactions, including limestone assimilation. However, none of the principal mineral constituents of the common calciocarbonatite melt are congruent at geologically reasonable temperatures and crustal pressures. In silicocarbonatite magmatic systems, decarbonation reactions may be dominant. At high temperature, the reaction $CaMg(CO_3)_2 \Rightarrow MgO + CaCO_3 + CO_2$ explains the presence of periclase. Periclase may react with the silicate melt component to generate pure forsterite $2MgO + SiO_2 \Rightarrow Mg_2SiO_4$, which exceeds the mantle *Mg#*. Olivine with low Ni + Cr, thus different from mantle debris, and very high *Mg#* may have been formed by this transient periclase-consuming reaction. Another Ca-rich form of olivine, monticellite $CaMgSiO_4$, is a common mineral, typical of early stage carbonatites (Hogarth, 1989), occurring as rims around olivine and clinopyroxene (Barker, 1989). Euhedral crystals or reaction rims of monticellite around mantle forsterite are widespread in Italian silicocarbonatites (Fig. 2h). The reaction $Mg_2SiO_4 + CaCO_3 = CaMgSiO_4 + MgO + CO_2$ explains the formation of monticellite at high temperatures and crustal pressures. A similar reaction, producing andradite garnet $Ca_3Fe_2(SiO_4)_3$ which forms rims around mafic crystals in the Ficoreto tuffisite, may be written as $3CaCO_3 + Fe_2O_3 + 3SiO_2 = Ca_3Fe_2(SiO_4)_3 + 3CO_2$. Silicate saturation experiments show low SiO_2-solubility in carbonatite melts, even at high temperatures; such reactions involving carbonate and silicate minerals should probably be peritectic and conserve SiO_2 contents in the carbonatite melt (Weidendorfer et al., 2017). Calcite with pseudo-hexagonal morphology, a feature of RR carbonatites, can best be explained as a pseudomorph after aragonite. The stability limit of an aragonite-bearing carbonatite melt extends from ~1100 °C (at ~30 kbar at the base of the lithosphere) to asthenospheric temperatures and pressures (Wyllie and Boettcher, 1969). The minimum pressure of the aragonite solidus substantially exceeds the crustal lithostatic load, thus favouring crystallisation of the aragonite in the mantle above the local geotherm. However, aragonite is not stable at high T and low P and requires hydraulic over-pressurisation, possibly produced in the magmatic convoy by saturation with CO_2 globules confined in a narrow conduit, or propagating dykes, after diatresis. Near-surface CO_2 decompression causes the metastable aragonite phenocrysts to quench in the calcite stability field at low P and T, preserving a pseudo-hexagonal shape (Hurai et al., 2013), although very rarely aragonite survives as inclusions in mantle olivine from carbonatite tuffs (e.g. Calatrava; Humphreys et al., 2010).

The liquid temperature of carbonatite varies from 800 to 1200 °C, at crustal pressure, and the melt is stable in this temperature range (Durand et al., 2015). Crystallisation of fluor-calciocarbonatite may, in orthomagmatic conditions, be at a temperature near 875 °C, according to the phase diagram CaF_2-$CaCO_3$ (Gittins and Tuttle, 1964). Calcite is in the liquidus phase at temperatures > 800 °C in a system K_2CO_3–$CaCO_3$ and with additional fluorine this temperature drops to < 600 °C, approaching the peritectic point nyererite + cc – L + cc (Jago and Gittins, 1991; Cooper et al., 1975). Fluorellestadite ± periclase inclusions both in calcite microphenocrysts and in the
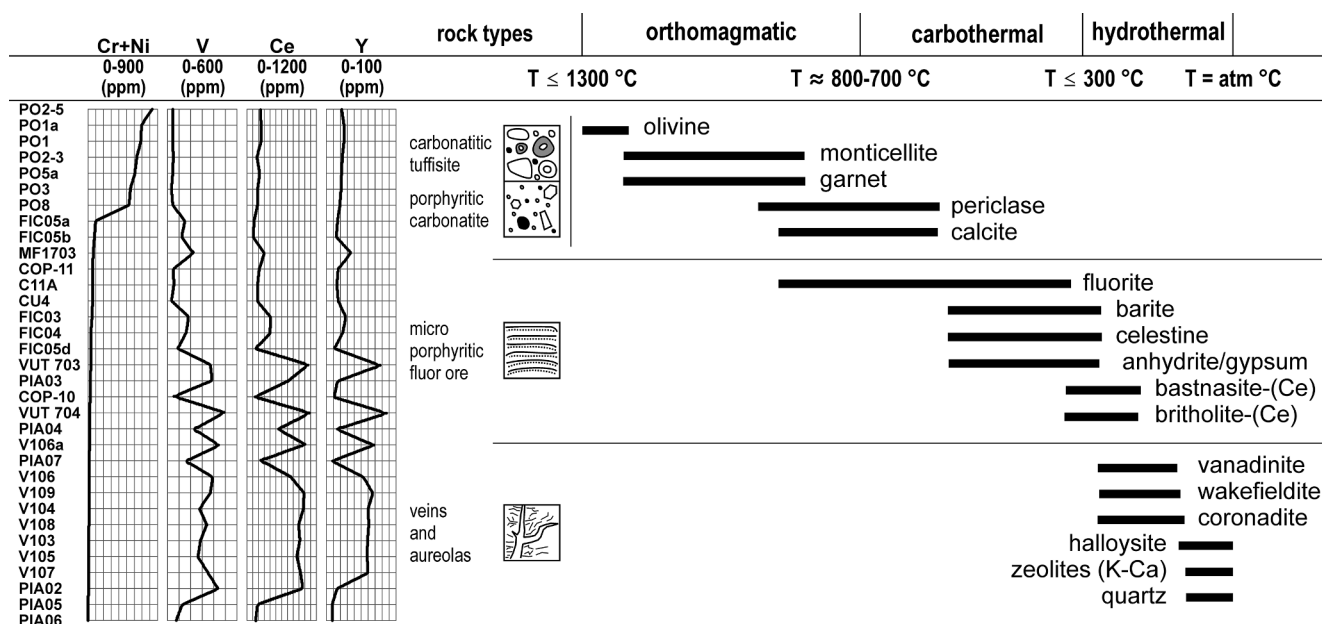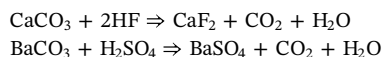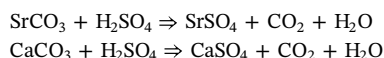
Fig. 10. Synoptic scheme of carbonatite, fluor-calciocarbonatite and fluor ore deposits textural and mineralogical features. Mineral stable assemblages are deduced by experimental petrology literature and textural observation. Distribution of specific critical metals in function of decreasing compatible metals are also displayed.

groundmass at Pianciano and Ficoreto suggest precipitation at 700 to 800 °C, by analogy with periclase marble (Kokh et al., 2015).

In carbothermal conditions below orthomagmatic temperatures but above H_2O critical temperatures, the REEs preferentially enter apatite, hellestadite and britholite. At this stage, REEs form complexes with CO_3^{2-}, SO_4^{2-}, and F^- ligands (Liu and Hou, 2017; Liu et al., 2018; Zheng and Liu, 2019; Shu and Liu, 2019). $LFSE^{2+}$ increases by orders of magnitude and precipitates, mostly as sulphates. Sulphate minerals may precipitate together with fluorite, according to the reactions

$$CaCO_3 + 2HF \Rightarrow CaF_2 + CO_2 + H_2O$$
$$BaCO_3 + H_2SO_4 \Rightarrow BaSO_4 + CO_2 + H_2O$$

or

$$SrCO_3 + H_2SO_4 \Rightarrow SrSO_4 + CO_2 + H_2O$$
$$CaCO_3 + H_2SO_4 \Rightarrow CaSO_4 + CO_2 + H_2O$$

These reactions predict a drastic increase of the $H_2O + CO_2/F_2$ ratio value. The breakdown of LREE-enriched calcite in the reaction above could provide a source of LREE to produce a succession of lower temperature REE-minerals. The theoretical solubility products for fluorides are higher for Y and HREE than for LREE (Migdisov et al., 2009; Tropper et al., 2011); hence, sulphate complexation has an important role to play in the Y-concentration in fluorite. Critically, fluorine behaves differently depending on the cooling rate (subvolcanic/volcanic), CO_2 abundance and the availability of water in mixed COHF fluid systems. Subvolcanic cooling conditions favour precipitation of $HSFE^{4+5+}$ in the silicate fraction, whereas $LFSE^{2+}$ and $HFSE^{2+3+}$ are concentrated in the carbothermal residua (Figs. 5 and 6) (Lowenstern, 2001; Bühn et al., 2002).

4.4. Hydrothermal stage

The hydrothermal stage may be divided into high-, medium-T (350–200 °C, H_2O vapour) and low-T (< 200 °C, juvenile water) hydrothermal stages. Due to the increase of REE and Y passing from fluor-calciocarbonatite to fluor ore, we assume that the solubility of REEs and Y in F-bearing fluids increases with decreasing temperature. There is not experimental support about that, but it could be easily tested with future laboratory reaction experiments. Crystallisation of REE-fluor-carbonates is favoured in the high-T hydrothermal stage, by the
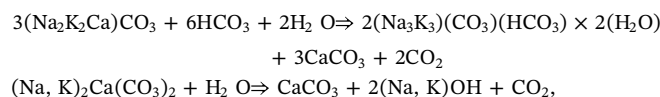
previous massive precipitation of fluorite–barite–calcite as gangue minerals in the carbothermal stage, and this removes the REE-stabilizing ligands F^-, $(SO4)^{2-}$, and $(CO3)^{2-}$ in the ore-fluids. The source and balance of energy in this system, i.e. chemical, mechanical, thermal, may be sufficient to produce a vigorous 'hydrothermal ascent' phase moving towards the surface, producing eruption of the system (Stoppa et al., 2016) and the complex fracture/intrusion system observed, for example, at Pianciano and Ficoreto. Homogenisation temperatures (~250–350 °C) of fluid inclusions in bastnäsite suggest that at the high-T hydrothermal stage (Shu and Liu, 2019), CO_2 exsolution may still have an important role to play in mineralisation: $REEF^{2+} + CO_3^{2-} = REE(CO_3)F$ (bastnäsite) (Hou et al., 2015; Liu and Hou, 2017). Vanadinite, wakefieldite and many other REE-minerals (i.e. ciprianiite) also precipitate at this stage (Guo and Liu, 2019).

Deposition in multiple generations of pervasive veins supports the idea that the fluorite, quite pure calcite, gypsum, celestine, quartz, analcime, halloysite and zeolite mineral assemblage does not represent in situ alteration of previous rocks as suggested by Di Sabatino et al. (1979). Substitution of Na^+ for K^+ and hydration explains the transformation of leucite into analcime. Analcime may then be transformed into halloysite and quartz:

$$2Na(AlSi_2O_6)H_2 O + 2HF = Al_2(Si_2O_5)(OH)_4 + 2NaF + H_2 O + 2SiO_2.$$

This reaction requires a change of K^+/H^+ and high Na^+/H^+, producing a transition from leucite to analcime and, at low or negative ratios, precipitates to halloysite in the low-T hydrothermal stage (Savage et al., 2001). In low-T hydrothermal conditions, hydroxyl-bastnäsite and hydroxyl-wakefieldite and other Ce-V-hydroxylated phases also precipitate, and this has, hitherto, only been described from pegmatites (Guastoni et al., 2009, 2010).

Alkaline igneous carbonates are very reactive and prone to recrystallise and re-equilibrate with the atmosphere and hydrosphere. External waters enter the crystallising system when the pressure in the fluid system changes from hydrostatic to lithostatic (descent phase). At low-T, alkaline elements preferentially complex as hydroxide or bicarbonate species in the presence of elevated pH_2O:

$$3(Na_2K_2Ca)CO_3 + 6HCO_3 + 2H_2 O \Rightarrow 2(Na_3K_3)(CO_3)(HCO_3) \times 2(H_2O) + 3CaCO_3 + 2CO_2$$
$$(Na, K)_2Ca(CO_3)_2 + H_2 O \Rightarrow CaCO_3 + 2(Na, K)OH + CO_2,$$

or

$$(Na, K)_2 Ca(CO_3)_2 + H_2O + CO_2 = CaCO_3 + 2(Na, K)HCO_3.$$

The phases illustrated as the products on the right hand side of the above reactions are readily soluble in water, and do not survive in the geological record (Wall, 2004).

5. Conclusions

In terms of mineralogy, trace element geochemistry and isotope geochemistry, Italian carbonatites show compositional ranges that are compatible with chemical immiscibility. After separation from the main silicate component, carbonatite en route to the surface evolves by progressive decarbonation. We emphasise the role of mantle debris in the magma evolution by means of silicate-carbonate reactions. The breakdown reaction of former dolomite explains the presence of periclase. These phenomena account for the transformation of the primary silicomagnesiocarbonatite melts into silicocalciocarbonatite magmas. The physical-chemical peculiarities of the melt enabled a sequence of carbonate-silicate reactions to crystallise near end-member forsterite, andradite garnet and monticellite olivine, which are distinctive.

The Italian carbonatites exhibit important and localised outcrop textures characterised by pelletal lapilli, which are typical of tuffisites, considered to represent a subvolcanic natural mixture of silicate and carbonate components generated by energetic CO_2 exsolution from mantle lithospheric levels through propulsion in a crustal-dissecting narrow conduit (diatreme). Textural and chemical equilibrium between carbonatite and associated silicate rocks favours immiscibility over crystal fractionation and assimilation, which are difficult in high velocity magma propagation. Very high $Mg\#$ and $Cr + Ni$, mantle xenoliths and xenocrysts, experimental petrology inferences and statistical calculation all suggest that primitive Italian carbonatites are derived from a CO_2-rich alkaline magma by immiscibility. Mineral-hosted inclusions indicate that, at the magmatic stage, nyerereite co-crystallised with calcite. Primary melt may come up from a subasthenospheric deep mantle level.

We remark that Italian carbonatites are not just very primitive, mantle nodules bearing but also evolved carbonatite and (carbo) hydrothermal system too. Large volumes of fluor-calciocarbonatite formed during the orthomagmatic stage when calcite, fluorite and barite formed stable mineral assemblages at magmatic temperatures ($> 800\,°C$). Cotectic crystallization of fluorite and calcite is strictly associated with immiscibility and has been documented by several authors (e.g. Panina, 2005) and discussed by Kynicky et al. (2018). We conclude that fluorine concentration is related to late evolution of the melt that produces fluor calciocarbonatites, syenites and, finally, fluor ore.

CO_2, H_2O, S and F concentrate at the carbothermal stage, which is equivalent to a pegmatitic stage. Upon passage from the orthomagmatic to the carbothermal stage, fluorite and barite (as well as celestine and anhydrite) precipitate, forming fluor-calciocarbonatite. The REE patterns of minerals give a measure of thermal and compositional evolution (Fig. 10) and show progressively stronger and more pronounced LREE enrichment, coupled with high concentrations of V, Cs, Pb, Sr, and Ba. Alkaline carbonate minerals, complexed as hydroxide or bicarbonate species, recede with the loss of hydrous fluids.

The solubility of REEs and Y- in F-bearing fluids increases at the high-T, hydrothermal stage. Bastnäsite, vanadinite, wakefieldite and many other ore-forming minerals precipitate at this stage. This multi-stage model is not entirely new or specific to the Italian carbonatitic system, but is quite similar to those in Maoniuping and Dalucao (Liu and Hou, 2017) and Pianciano fluor ore and fluor calciocarbonatite have very similar compositions to Lizhuang bastnäsite-bearing calcite, fluorite and barite ore (Liu and Hou, 2017) and Amba Dongar (Viladkar et al., 2019).

Sr–Nd isotopic compositions suggest a co-participation of an extremely enriched mantle component ITEM. Fractionation, operated by high-temperature CO_2 exsolution, explains the elevated $\delta^{18}O$ and negative $\delta^{13}C$ recognised in Italian carbonatites. The heavy C isotopic signature requires open-system fractionation at near magmatic temperatures ($> 500\,°C$).

To summarise, the geology and geochemistry of Italian carbonatites convincingly depicts the following scenario:

1. Partial melting of a metasomatised mantle forms primary CO_2-rich ultra-alkaline magma (silicomagnesiocarbonatite).
2. Violent deep exsolution of CO_2 propels the magmatic convoy towards the surface.
3. Immiscibility produces conjugate carbonatite and silicate ultra-alkaline melts.
4. Decarbonation reactions occur at crustal level with intense CO_2 release.
5. Carbothermal fluids, rich in F-S-P, precipitate fluorite, barite and REE fluorphosphates.
6. The hydrothermal stage precipitates hydrated variants of bastnäsite, wakefieldite, vanadinite and coronadite.
7. Fluor-calciocarbonatite probably exsolved-fractionated the associated fluor ore during a carbothermal stage and was then modified by hydrothermalism, so fluor-calciocarbonatites can also be a useful exploration tool for high-grade REE-ore.

We are confident that the extensive arguments we have documented across Italy (RR, IUP etc.) and their agreement with systematic global carbonatites, and laboratory experiments, provide a sound basis for a petrogenetic model that requires a primary carbonate presence in the parental melt of the ultra-alkaline rocks of Italy. The presence of carbonatites in the RR makes limestone assimilation unnecessary because carbonate was already present in the RR parental melts as a primary component.

This model may be generalised for use with worldwide carbonatites associated with alkaline rocks and REE (and fluorite) ores, and could be easily tested with future laboratory reaction experiments. This paper offers a model that changes the way we think about the Italian carbonatites. It implies that the RR fluor-calciocarbonatites and fluor ore are produced by a decarbonation reaction and volatile (CO_2, F, S) concentration after separation of calciocarbonatite from melilite leucitite melt. Further low-temperature processes precipitate REE minerals. This completes the previous petrogenitic model for IUP primitive silicocarbonatites based on rapid propagation by diatremic fluidification.

Appendix A. Supplementary data

Supplementary data to this article can be found online at https://doi.org/10.1016/j.oregeorev.2019.103041.

References

Al-Ali, S., Wall, F., Sheridan, R., Pickles, J., Pascoe, R., 2019. Magnetic properties of REE fluorcarbonate minerals and their implications for minerals processing. Miner. Eng. 131, 392–397. https://doi.org/10.1016/j.mineng.2018.11.042.

Bailey, D.K., 1985. Fluids, melts, flowage, and styles of eruption in alkaline – ultra-alkaline magmatism. Transact. Trans. Geol. Soc. S. Afr. 88, 449–457.

Barker, D.S., 1989. Field relations of carbonatites. In: Bell, K. (Ed.), Carbonatites: Genesis and Evolution. Unwin Hyman, London.

Bell, K., Kjarsgaard, B.A., 2006. Discussion of Peccerillo (2004) "Carbonate-rich pyroclastic rocks from central apennines: carbonatites or carbonated rocks?". Period. Mineral. 75 (1), 85–92.

Bell, K., Lavecchia, G., Rosatelli, G., 2013. Cenozoic Italian magmatism - Isotope constraints for possible plume-related activity. J. S. Am. Earth Sci. 41, 22–40. https://doi.org/10.1016/j.jsames.2012.10.005.

Brocchini, D., Di Battistini, G., Laurenzi, M.A., Vernia, L., 2000. New 40Ar/39Ar datings on the Southeastern sector of the Vulsinian Volcanic District (Central Italy). Boll. Soc. Geol. Ital. 119, 113–120.

Brod, J.A., Junqueira-Brod, T.C., Gaspar, J.C., Petrinovic, I.A., Valente, S.C., Corval, A., 2013. Decoupling of paired elements, crossover REE patterns, and mirrored spider diagrams: fingerprinting liquid immiscibility in the Tapira alkaline-carbonatite complex, SE Brazil. J. S. Am. Earth Sci. 41, 41–56. https://doi.org/10.1016/j.jsames.2012.04.013.

Brooker, R.A., Kjarsgaard, B.A., 2011. Silicate-Carbonate Liquid Immiscibility and Phase Relations in the System SiO2–Na2O–Al2O3–CaO–CO2 at 0·1–2·5 GPa with Applications to Carbonatite Genesis. J. Petrol. 52, 1281–1305. https://doi.org/10.1093/petrology/egq081.

Bühn, B., Rankin, A.H., Schneider, J., Dulskic, P., 2002. The nature of orthomagmatic, carbonatitic fluids precipitating REE, Sr-rich fluorite: fluid-inclusion evidence from the Okorusu fluorite deposit, Namibia. Chem. Geol. 186, 75–98. https://doi.org/10.1016/S0009-2541(01)00421-1.

Campeny, M., Mangas, J., Melgarejo, J.C., Bambi, A., Alfonso, P., Gernon, T., Manuel, J., 2014. The Catanda extrusive carbonatites (Kwanza Sul, Angola): an example of explosive carbonatitic volcanism. Bull. Volcanol. 76 (4), 1–15. https://doi.org/10.1007/s00445-014-0818-6.

Carmichael, I.S.E., 1964. Natural liquids and the phonolitic minimum. Geol. J. 4, 55–60.

Castorina, F., Stoppa, F., Cundari, A., Barbieri, M., 2000. An enriched mantle source for Italy's melilitite-carbonatite association as inferred by its Nd-Sr isotope signature. Mineral. Mag. 64, 625–639. https://doi.org/10.1180/002646100549652.

Chacko, T., Mayeda, T.K., Clayton, R.N., Goldsmith, J.R., 1991. Oxygen and carbon isotope fractionations between CO2 and calcite. Geochim. Cosmochim. Acta 55 (10), 2867–2882. https://doi.org/10.1016/0016-7037(91)90452-B.

Chakhmouradian, A.R., 2006. High-field-strength elements in carbonatitic rocks: geochemistry, crystal chemistry and significance for constraining the sources of carbonatites. Chem. Geol. 235 (1–2), 138–160. https://doi.org/10.1016/j.chemgeo.2006.06.008.

Cooper, A.F., Gittins, J., Tuttle, O.F., 1975. The system Na2CO3-K2CO3-CaCO3 at 1 kilobar and its significance in carbonatite petrogenesis. Am. J. Sci. 275, 534–560.

Cozzupoli, D., Federico, M., Fornaseri, M., 1976. Mineralizzazione calcitico-apatitica-fluoritica in giacituta filoniana in un cono di scorie presso Sacrofano (Regione Sabazia). Rend. Soc. Ital. Mineral. Petrol. 32, 197–214.

Cundari, A., Ferguson, A.K., 1991. Petrogenetic relationships between melilitite and lamproite. Contrib. Miner. Petrol. 107, 343–357. https://doi.org/10.1007/BF00325103.

Dalton, J.A., Wood, B.J., 1993. The compositions of primary carbonate melts and their evolution through wallrock reaction in the mantle. Earth Planet. Sci. Lett. 119, 511–525. https://doi.org/10.1016/0012-821X(93)90059-I.

Deans, T., Powell, J.L., 1968. Trace elements and strontium isotopes in carbonatites fluorites, and limestones from India and Pakistan. Nature 218, 750–752. https://doi.org/10.1038/218750a0.

Deines, P., 1989. Stable isotope variations in carbonatites. In: Bell, K. (Ed.), Carbonatites: Genesis and Evolution. Unwin Hyman, London.

Demény, A., Harangi, S., 1996. Stable isotope studies and processes of carbonate formation in Hungarian alkali basalts and lamprophyres: evolution of magmatic fluids and magma-sediment interactions. Lithos 37 (4), 335–349. https://doi.org/10.1016/0024-4937(95)00029-1.

Demény, A., Forizs, I., Molnar, F., 1994. Stable isotope and chemical compositions of carbonate ocelli and veins in Mesozoic lamprophyres of Hungary. Eur. J. Mineral. 6 (5), 679–690. https://doi.org/10.1127/ejm/6/5/0679.

Di Battistini, G., Montanini, A., Vernia, L., Venturelli, G., Tonarini, S., 2001. Petrology of melilite-bearing rocks from the Montefiascone Volcanic Complex (Roman Magmatic Province): new insights into the ultrapotassic volcanism of Central Italy. Lithos 59, 1–24. https://doi.org/10.1016/S0024-4937(01)00054-8.

Di Sabatino, B., Barrese, E., Giampaolo, C., 1979. Sulla genesi delle fluoriti "sedimentarie" area meridionale del sistema vulcanico sabatino. Rend. Soc. Ital. Mineral. Petrol. 35 (1), 439–451.

Doroshkevich, A.G., Ripp, G.S., Viladkar, S.G., Vladykin, N.V., 2008. The Arshan REE carbonatites, southwestern Transbaikalia, Russia: mineralogy, paragenesis and evolution. Can. Mineral. 46 (4), 807–823. https://doi.org/10.3749/canmin.46.4.807.

Downes, H., Kostoula, T., Jones, A.P., Beard, A.D., Thirlwall, M.F., Bodinier, J.-L., 2002. Geochemistry and Sr–Nd isotopic compositions of mantle xenoliths from the Monte Vulture carbonatite–melilitite volcano, central southern Italy. Contrib. Miner. Petrol. 144, 78–92. https://doi.org/10.1007/s00410-002-0383-4.

Durand, C., Baumgartner, L.P., Marquer, D., 2015. Low melting temperature for calcite at 1000 bars on the join CaCO3-H2O - some geological implications. Terra Nova 27 (5), 364–369. https://doi.org/10.1111/ter.12168.

Eriksson, S.C., 1989. Phalaborwa: a saga of magmatism, metasomatism and miscibility. In: Bell, K. (Ed.), Carbonatites: Genesis and Evolution. Unwin Hyman, London, pp. 221–250.

Francis, E.H., 1989. Tuffisite. Petrology. Encyclopedia of Earth Science. Springer, Boston, MA.

Gambardella, B., Cardellini, C., Chiodini, G., Frondini, F., Marini, L., Ottonello, G., Vetuschi Zuccolini, M., 2004. Fluxes of deep CO2 in the volcanic areas of Central-Southern Italy. J. Volcanol. Geoth. Res. 136, 31–52. https://doi.org/10.1016/j.jvolgeores.2004.03.018.

Gittins, J., Tuttle, O.F., 1964. The system CaF2-Ca(OH)2-CaCO3 and the origin of carbonatites. Am. J. Sci. 262, 66–75.

Goodenough, K.M., Schilling, J., Jonsson, E., Kalvig, P., Charles, N., Tuduri, J., Deady, E.A., Sadeghi, M., Schiellerup, V., Müller, A., Bertrand, G., Arvanitidis, N., Eliopoulos, D.G., Shaw, R.A., Thrane, K., Keulen, N., 2016. Europe's rare earth element resource potential: an overview of REE metallogenetic provinces and their geodynamic setting. Ore Geol. Rev. 72 (1), 838–856. https://doi.org/10.1016/j.oregeorev.2015.09.019.

Guastoni, A., Nestola, F., Giaretta, A., 2009. Mineral chemistry and alteration of rare earth element (REE) carbonates from alkaline pegmatites of Mount Malosa, Malawi. Am. Mineral. 94 (8–9), 1216–1222. https://doi.org/10.2138/am.2009.3185.

Guastoni, A., Kondo, D., Nestola, F., 2010. Bastnäsite-(Ce) and parisite-(Ce) from Mt. Malosa, Malawi. Gems Gemol. 46, 42–47.

Gudfinnsson, G.H., Presnall, D.C., 2005. Continuous gradations among primary carbonatitic, kimberlitic, melilititic, basaltic, picritic, and komatiitic melts in equilibrium with garnet lherzolite at 3–8 GPa. J. Petrol. 46 (8), 1645–1659. https://doi.org/10.1093/petrology/egi029.

Guo, D.X., Liu, Y., 2019. Occurrence and geochemistry of bastnäsite in carbonatite-related REE deposits, Mianning-Dechang REE belt, Sichuan Province, SW China. Ore Geol. Rev. 107, 266–282. https://doi.org/10.1016/j.oregeorev.2019.02.028.

Gupta, A.K., Yagi, K., 1980. Petrology and genesis of leucite-bearing rocks. In: Minerals and Rocks. Springer-Verlag, , Berlin, New York, XIV, pp. 252.

Hogarth, D.D., 1989. Pyrochlore, apatite and amphibole - distinctive minerals in carbonatite. In: Bell, K. (Ed.), Carbonatites: Genesis and Evolution. Unwin Hyman, London.

Hou, Z.Q., Liu, Y., Tian, S.H., Yang, Z.M., Xie, Y.L., 2015. Formation of carbonatite-related giant rare-earth-element deposits by the recycling of marine sediments. Sci. Rep. 10231. https://doi.org/10.1038/srep10231.

Humphreys, E.R., Bailey, K., Hawkesworth, C., Wall, F., Najorka, J., Rankin, A.H., 2010. Aragonite in olivine from Calatrava, Spain-Evidence for mantle carbonatite melts from > 100 km depth. Geology 38 (10), 911–914. https://doi.org/10.1130/G31199.1.

Hurai, V., Huraiová, M., Milovský, R., Luptáková, J., Konečný, P., 2013. High-pressure aragonite phenocrysts in carbonatite and carbonated syenite xenoliths within an alkali basalt. Am. Mineral. 98 (5–6), 1074–1077. https://doi.org/10.2138/am.2013.4410.

Isakova, A.T., Panina, L.I., Stoppa, F., 2017. Genesis of kalsilite melilitite at Cupaello, Central Italy: evidence from melt inclusions. Petrology 25, 433–447. https://doi.org/10.1134/S0869591117040038.

Isakova, A.T., Panina, L.I., Stoppa, F., 2019. Formation conditions of leucite-bearing lavas in the bolsena complex (Vulsini, Italy): research data on melt inclusions in minerals. Russ. Geol. Geophys. 60 (2), 119–132. https://doi.org/10.15372/RGG2019009.

Jago, B., Gittins, J., 1991. The role of fluorine in carbonatite magma evolution. Nature 349, 56–58. https://doi.org/10.1038/349056a0.

Jones, A.P., Wall, F., Williams, C.T., 1996. Rare earth minerals: chemistry, origin and ore deposits. In: The Mineralogical Society Series. Springer, Netherlands, pp. 372.

Jones, A.P., Kostoula, T., Stoppa, F., Woolley, A.R., 2000. Petrography and mineral chemistry of mantle xenoliths in a carbonate-rich melilititic tuff from Mt. Vulture volcano, southern Italy. Mineral. Mag. 64, 593–613. https://doi.org/10.1180/002646100549634.

Jones, A.P., Genge, M., Carmody, L., 2013. Carbonate melts and carbonatites. Rev. Mineral. Geochem. 75 (1), 289–322. https://doi.org/10.2138/rmg.2013.75.10.

Kokh, S.N., Sokol, E.V., Sharygin, V.V., 2015. Ellestadite-group minerals in combustion metamorphic rocks. In: Stracher, G.B., Prakash, A., Sokol, E.V. (Eds.), Coal and Peat Fires: A Global Perspective: Case Studies - Coal Fires, pp. 543–562. https://doi.org/10.1016/B978-0-444-59509-6.00020-X.

Kynicky, J., Smith, M.P., Wenlei, S., Chakhmouradian, A., Xu, C., Kopřiva, A., Vasinova, G.M., Brtnický, M., 2018. The role of carbonate-fluoride melt immiscibility in shallow REE deposit evolution. Geosci. Front. 10 (2), 527–537. https://doi.org/10.1016/j.gsf.2018.02.005.

Lavecchia, G., Stoppa, F., 1996. The tectonic significance of Italian magmatism: an alternative view to the popular interpretation. Terra Nova 8 (5), 435–446. https://doi.org/10.1111/j.1365-3121.1996.tb00769.x.

Lavecchia, G., Creati, N., Boncio, P., 2002. The Intramontane Ultra-alkaline Province (IUP) of Italy: a brief review with considerations on the thickness of the underlying lithosphere. Boll. Soc. Geol. Ital. 1, 87–98.

Lavecchia, G., Stoppa, F., Creati, N., 2006. Carbonatites and kamafugites in Italy: mantle-derived rocks that challenge Subduction. In: Scalera, G., Lavecchia, G. (Eds.), Frontiers in Earth Sciences: New Ideas and Interpretation. Ann. Geophys-Italy, pp. 389–402.

Lavecchia, G., Adinolfi, G.M., De Nardis, R., Ferrarini, F., Cirillo, D., Brozzetti, F., De Matteis, R., Festa, G., Zollo, A., 2017. Multidisciplinary inferences on a newly recognized active east-dipping extensional system in Central Italy. Terra Nova 29, 77–89. https://doi.org/10.1111/ter.12251.

Liu, Y., Hou, Z.Q., 2017. A synthesis of mineralization styles with an integrated genetic model of carbonatite-syenite-hosted REE deposits in the Cenozoic Mianning-Dechang REE metallogenic belt, the eastern Tibetan Plateau, southwestern China. J. S. Am. Earth Sci. 137, 35–79. https://doi.org/10.1016/j.jseaes.2017.01.010.

Liu, Y., Chakhmouradian, A.R., Hou, Z.Q., Song, W.L., Kynický, J., 2018. Development of

REE mineralization in the giant Maoniuping deposit (Sichuan, China): insights from mineralogy, fluid inclusions, and trace-element geochemistry. Miner. Deposita 54, 701–718. https://doi.org/10.1007/s00126-018-0836-y.

Lloyd, F.E., Stoppa, F., 2003. Pelletal lapilli in diatremes - some inspiration from the old masters. Geolines 15, 65–71.

Locardi, E., 1990. Le mineralizzazioni fluoritifere laziali sono dei carbonatiti: l'esempio di Pianciano. L'Ind. Miner. 6, 1–7.

Lowenstern, J.B., 2001. Carbon dioxide in magmas and implications for hydrothermal sytems. Miner. Deposita 36, 490–502. https://doi.org/10.1007/s001260100185.

Lyubetskaya, T., Korenaga, J., 2007. Chemical composition of Earth's primitive mantle and its variance: 1. Method and results. J. Geophys. Res. 112, B03211. https://doi.org/10.1029/2005JB004223.

Martin, L.H., Schmidt, M.W., Mattsson, H.B., Ulmer, P., Hametner, K., Günther, D., 2012. Element partitioning between immiscible carbonatite–kamafugite melts with application to the Italian ultrapotassic suite. Chem. Geol. 320, 96–112. https://doi.org/10.1016/j.chemgeo.2012.05.019.

Martin, L.H.J., Schmidt, M.W., Mattsson, H.B., Guenther, D., 2013. Element partitioning between immiscible carbonate and silicate melts for dry and H$_2$O-bearing systems at 1–3gpa. J. Petrol. 54 (11), 2301–2338. https://doi.org/10.1093/petrology/egt048.

Masi, U., Turi, B., 1971. La composizione isotopica dell'ossigeno e del carbonio del carbonato presente nei depositi calcitico-fluoritici pleistocenici dei Colli della Farnesina (Roma) e di Colle di Pianciano (Bracciano). Period. Mineral. 40, 213–240.

Masi, U., Turi, B., 1976. Composizione isotopica del carbonato di una mineralizzazione a calcite, apatite e fluorite in vene nel cono di scorie pleistocenico di monte Ficoreto, presso Sacrofano (regione sabazia orientale, Lazio). Rend. Soc. Ital. Mineral. Petrol. 32, 261–271.

Mastrangelo, F., 1976. I giacimenti. Rend. Soc. Ital. Mineral. Petrol. 32, 29–46.

Mattey, D.P., Taylor, W.R., Green, D.H., Pillinger, C.T., 1990. Carbon isotopic fractionation between CO$_2$ vapour, silicate and carbonate melts: an experimental study to 30 kbar. Contrib. Miner. Petrol. 104, 492–505. https://doi.org/10.1007/BF01575626.

Migdisov, A.A., Williams-Jones, A.E., Wagner, T., 2009. An experimental study of the solubility and speciation of the Rare Earth Elements (III) in fluoride- and chloride-bearing aqueous solutions at temperatures up to 300 ˚C. Geochim. Cosmochim. Acta 73, 7087–7109. https://doi.org/10.1016/j.gca.2009.08.023.

Mitchell, R.H., 2005. Carbonatites and carbonatites. Can. Mineral. 43, 2049–2068. https://doi.org/10.2113/gscanmin.43.6.2049.

Nelson, D.R., Chivas, A.R., Chappell, B.W., McCulloch, M.T., 1988. Geochemical and isotopic systematics in carbonatites and implications for the evolution of ocean-island sources. Geochim. Cosmochim. Acta 52, 1–17. https://doi.org/10.1016/0016-7037(88)90051-8.

Panina, L., 2005. Multiphase carbonate-salt immiscibility in carbonatite melts: Data on melt inclusions from the Krestovskiy massif minerals (Polar Siberia). Contrib. Mineral. Petr. 150 (1), 19–36. https://doi.org/10.1007/s00410-005-0001-3.

Panina, L.I., Stoppa, F., Usol'tseva, L.M., 2003. Genesis of melilitite rocks of Pian di Celle volcano, umbrian kamafugite province, Italy: evidence from melt inclusions in minerals. Petrology 11 (4), 365–382.

Pearce, J.A., 2008. Geochemical fingerprinting of oceanic basalts with applications to ophiolite classification and the search for Archean oceanic crust. Lithos 100, 14–48. https://doi.org/10.1016/j.lithos.2007.06.016.

Peccerillo, A., 2016. In: Cenozoic Volcanism in the Tyrrhenian Sea Region. Springer, pp. 399. https://doi.org/10.1007/978-3-319-42491-0.

Petrov, T.G., Krasnova, N.I., Balaganskaya, E., Moutte, J., 2016. The RHA Method. https://www.emse.fr/~moutte/rha/.

Petrov, T.G., Moshkin, S.V., 2015. Method RHAT and its implementation in the software package Petros-3. In: Modern Information Technologies, pp. 70–80.

Presnall, D., Gudfinnsson, G.H., 2005. Carbonate-rich melts in the oceanic low-velocity zone and deep mantle. In: Foulger, G.R., Natland, J.H., Presnall, D.C., Anderson, D.L. (Eds.), Plates, plumes and paradigms. Spec. Pap. - Geol. Soc. Am. pp. 207–216. https://doi.org/10.1130/0-8137-2388-4.207.

Rosatelli, G., Wall, F., Stoppa, F., 2007. Calcio-carbonatite melts and metasomatism in the mantle beneath Mt. Vulture (Southern Italy). Lithos 99, 229–248. https://doi.org/10.1016/j.lithos.2007.05.011.

Rosatelli, G., Wall, F., Stoppa, F., Brilli, M., 2010. Geochemical distinctions between igneous carbonate, calcite cements, and limestone xenoliths (Polino carbonatite, Italy): spatially resolved LAICPMS analyses. Contrib. Miner. Petrol. 160, 645–661. https://doi.org/10.1007/s00410-010-0499-x.

Santos, R.V., Clayton, R.N., 1995. Variations of oxygen and carbon isotopes in carbonatites: a study of Brazilian alkaline complexes. Geochim. Cosmochim. Acta 59, 1339–1352. https://doi.org/10.1016/0016-7037(95)00048-5.

Savage, D., Rochelle, C., Moore, Y., Milodowski, A., Bateman, K., Bailey, D., Mihara, M., 2001. Analcime reaction at 25–90 ˚C in hyperalkaline fluids. Mineral. Mag. 65 (5), 571–588. https://doi.org/10.1180/002646101317018406.

Savelyeva, V.B., Demonterova, E.I., Danilova, Y.V., Bazarova, E.P., Ivanov, A.V., Kamenetsky, V.S., 2016. New carbonatite complex in the western Baikal area, southern Siberian craton: mineralogy, age, geochemistry, and petrogenesis. Petrology 24 (3), 271–302. https://doi.org/10.1134/S0869591116030061.

Sharygin, V.V., Pekov, I.V., Zubkova, N.V., Khomyakov, A.P., Stoppa, F., Pushcharovsky, D.Y., 2013. Umbrianite, K$_7$Na$_2$Ca$_2$[Al$_3$Si$_{10}$O$_{29}$]F$_2$Cl$_2$, a new mineral species from melilitolite of the Pian di Celle volcano, Umbria. Italy. Eur. J. Mineral. 25 (4), 655–669. https://doi.org/10.1127/0935-1221/2013/0025-2306.

Sharygin, V.V., Stoppa, F., Kolesov, B.A., 1996. Cuspidine in melilitolites of San Venanzo (Italy). Trans. (Doklady) Russ. Acad. Sci./Earth Sci. Sect. 349 (5), 747–775.

Shu, X.C., Liu, Y., 2019. Fluid Inclusion constraints on the hydrothermal evolution of the dalucao carbonatite-related REE deposit, Sichuan Province. China. Ore Geol. Rev. 107, 41–57. https://doi.org/10.1016/j.oregeorev.2019.02.014.

Simonetti, A., Bell, K., Viladkar, S.G., 1995. Isotopic data from the Amba Dongar

Carbonatite Complex, west-central India: evidence for an enriched mantle source. Chem. Geol. 122 (1–4), 185–198. https://doi.org/10.1016/0009-2541(95)00004-6.

Stoppa, F., 1996. The San Venanzo maar and tuff ring, Umbria, Italy: eruptive behaviour of a carbonatite-melilitite volcano. Bull. Volcanol. 57 (7), 563–577. https://doi.org/10.1007/BF00304440.

Stoppa, F., Cundari, A., 1995. A new Italian carbonatite occurrence at Cupaello (Rieti) and its genetic significance. Contrib. Miner. Petrol. 122, 275–288. https://doi.org/10.1007/s004100050127.

Stoppa, F., Lupini, L., 1993. Mineralogy and petrology of the Polino monticellite calcio-carbonatite (Central Italy). Mineral. Petrol. 49, 213–231. https://doi.org/10.1007/BF01164595.

Stoppa, F., Lloyd, F., Rosatelli, G., 2003. CO$_2$ as the virtual propellant of carbonatite-kamafugite conjugate pairs and the eruption of diatremic tuffisite. Period. Mineral. 72, 205–222.

Stoppa, F., Principe, C., 1998. Eruption style and petrology of a new carbonatitic suite from the Mt. Vulture (southern Italy): the Monticchio Lakes Formation. J. Volcanol. Geoth. Res. 80 (1–2), 137–153. https://doi.org/10.1016/S0377-0273(97)85659-4.

Stoppa, F., Schiazza, M., 2013. An overview of monogenetic carbonatitic magmatism from Uganda, Italy, China and Spain: volcanological and geochemical features. J. S. Am. Earth Sci. 41, 140–159. https://doi.org/10.1016/j.jsames.2012.10.004.

Stoppa, F., Schiazza, M., 2014. Extreme chemical conditions of crystallization of Umbrian melilitolites and wealth of rare, late stage/hydrothermal minerals. Cent. Eur. J. Geosci. 6 (4), 549–564. https://doi.org/10.2478/s13533-012-0190-z.

Stoppa, F., Sharygin, V.V., Cundari, A., 1997. New mineral data from the kamafugite-carbonatite association: The melilitolite from Pian di Celle, Italy. Miner. Petrol. 61 (1), 27–45. https://doi.org/10.1007/BF01172476.

Stoppa, F., Woolley, R.A., 1997. The Italian carbonatites: field occurrence, petrology and regional significance. Mineral. Petrol. 59, 43–67. https://doi.org/10.1007/BF01163061.

Stoppa, F., Rosatelli, G., Wall, F., Jeffries, T., 2005. Geochemistry of carbonatite–silicate pairs in nature: a case history from Central Italy. Lithos 85, 26–47. https://doi.org/10.1016/j.lithos.2005.03.020.

Stoppa, F., Jones, A.P., Sharygin, V.V., 2009. Nyerereite from carbonatite rocks at Vulture volcano: implications for mantle metasomatism and petrogenesis of alkali carbonate melts. Cent. Eur. J. Geosci. 1, 131–151. https://doi.org/10.2478/v10085-009-0012-9.

Stoppa, F., Pirajno, F., Schiazza, M., Vladykin, N.V., 2016. State of the art: Italian carbonatites and their potential for critical-metal deposits. Gondwana Res. 37, 152–171. https://doi.org/10.1016/j.gr.2016.07.001.

Sun, S., McDonough, W.F., 1989. Chemical and isotopic systematics of oceanic basalts: implications for mantle composition and processes. In: Saunders, A.D., Norry, M.J. (Eds.), Magmatism in Ocean Basins. Geological Society, London, Special Publications, pp. 313–345. https://doi.org/10.1144/GSL.SP.1989.042.01.19.

Sweeney, R.J., 1994. Carbonatite melt compositions in the earth's mantle. Earth Planet. Sci. Lett. 128, 259–270. https://doi.org/10.1016/0012-821X(94)90149-X.

Treiman, A.H., Essene, E.J., 1984. A periclase-dolomite-calcite carbonatite from the Oka complex, Quebec, and its calculated volatile composition. Contrib. Miner. Petrol. 85 (2), 149–157. https://doi.org/10.1007/BF00371705.

Tropper, P., Manning, C.E., Harlov, D.E., 2011. Solubility of CePO$_4$ monazite and YPO$_4$ xenotime in H$_2$O and H$_2$O–NaCl at 800 ˚C and 1 GPa: implications for REE and Y transport during high-grade metamorphism. Chem. Geol. 282, 58–66. https://doi.org/10.1016/j.chemgeo.2011.01.009.

Velde, D., Yoder, H.S., 1976. In: The Chemical Composition of Melilite-bearing Eruptive Rocks. Carnegie Institution of Washington Yearbook, pp. 574–580.

Vichi, G., Stoppa, F., Wall, F., 2005. The carbonate fraction in carbonatitic Italian lamprophyres. Lithos 85, 154–170. https://doi.org/10.1016/j.lithos.2005.03.025.

Viladkar, S., Magna, T., Rapprich, V., Hopp, J., Čejková, B., 2019. Nb-V-enriched sövites of the northeastern and eastern part of the Amba Dongar carbonatite ring dike, India. Geochemistry In press.

Wall, F., 2004. An illustration of the evolution and alteration of carbonatites using REE, Sr-rich carbonatites at Nkombwa, Zambia. Deep-seated magmatism: its sources and their relation to plume processes. In: Vladykin, N.V. (Ed.), Deep seated Magmatism. Its Sources and their Relation to Plume Processes. Institute of Geography SB RAS, Irkutsk–Ulan-Ude, pp. 48–67 ISBN 5-94797-046-5.

Wall, F., 2013. Critical metals handbook. In: Critical Metals Handbook, https://doi.org/10.1002/9781118755341.ch13.

Washington, H.S., 1906. In: The Roman Comagmatic RegionCarnegie Institution of Washington, pp. 199.

Weidendorfer, D., Schmidt, M.W., Mattsson, H.B., 2017. A common origin of carbonatite magmas. Geology 45, 507–510. https://doi.org/10.1130/G38801.1.

Wyllie, P.J., Boettcher, A.J., 1969. Liquidus phase relationships in the system CaCO3-CO2-H2O to 40 kbars pressure with petrological applications. Am. J. Sci. 267A, 489–508.

Ying, J., Zhou, X., Zhang, H., 2004. Geochemical and isotopic investigation of the Laiwu-Zibo carbonatites from western Shandong Province, China, and implications for their petrogenesis and enriched mantle source. Lithos 75 (3–4), 413–426.

Zaccarini, F., Stumpfel, E.F., Garuti, G., 2004. Zirconolite and Zr–Th–U minerals in chromitites of the Finero Complex, westeren Alps, Italy: evidences for carbonatite-type metasomastim in a subcontinental mantle plume. Can. Mineral. 42, 1825–1845.

Zaitsev, A.N., Keller, J., 2006. Mineralogical and chemical transformation of Oldoinyo Lengai natrocarbonatites. Tanzania. Lithos 91 (1–4), 191–207. https://doi.org/10.1016/j.lithos.2006.03.018.

Zheng, X., Liu, Y., 2019. Mechanisms of element precipitation in carbonatite-related rare-earth element deposits: evidence from fluid inclusions in the Maoniuping deposit, Sichuan Province, southwestern China. Ore Geol. Rev. 107, 218–238. https://doi.org/10.1016/j.oregeorev.2019.02.021.